A NOVEL MUTAGENIC SCREEN REVEALS A MODEL FOR INTERACTION BETWEEN THE BIOFILM REGULATORY PROTEINS NSPS AND MBAA IN VIBRIO CHOLERAE

A Thesis
By
ERIN CAMPBELL YOUNG

Submitted to the Graduate School
at Appalachian State University
in partial fulfillment of the requirements for the degree of
MASTER OF SCIENCE

August 2019
Department of Biology

A NOVEL MUTAGENIC SCREEN REVEALS A MODEL FOR INTERACTION BETWEEN THE BIOFILM REGULATORY PROTEINS NSPS AND MBAA IN VIBRIO CHOLERAE

A Thesis
By
ERIN CAMPBELL YOUNG
August 2019

APPROVED BY:

_____
Dr. Ece Karatan
Chairperson, Thesis Committee

_____
Dr. Cortney Bouldin
Member, Thesis Committee

_____
Dr. Darren Seals
Member, Thesis Committee

_____
Dr. Zack Murrell
Chairperson, Department of Biology

_____
Dr. Michael McKenzie
Dean, Cratis D. Williams School of Graduate Studies

Abstract

A NOVEL MUTAGENIC SCREEN REVEALS A MODEL FOR INTERACTION BETWEEN THE BIOFILM REGULATORY PROTEINS NSPS AND MBAA IN VIBRIO CHOLERAE

Erin Campbell Young
B.S., University of North Carolina at Chapel Hill
M.S., Appalachian State University

Chairperson: Dr. Ece Karatan

The regulation of the transition between a motile, planktonic state and biofilm-associated, sessile state is important to the lifecycle of the human pathogen *Vibrio cholerae*, which is responsible for the disease cholera. Certain environmental signals have been shown to affect the formation of biofilms for this bacterium. For example, polyamines are ubiquitous, organic molecules that play a role in the regulation of *V. cholerae* biofilm formation. *V. cholerae* detects the presence of these molecules and modifies its behavior through a putative signaling pathway composed of a periplasmic protein, NspS, and a transmembrane protein, MbaA, which has tandem cytoplasmic GGDEF and EAL domains. Previous studies have determined that the EAL domain of MbaA has phosphodiesterase activity and can break down the secondary messenger c-di-GMP, which is a positive regulator of biofilm formation. In this signal transduction pathway, NspS is hypothesized to interact with the periplasmic domain of MbaA to inhibit the phosphodiesterase activity of the cytoplasmic EAL domain. When NspS is bound by a polyamine, this alters the effect NspS has on the phosphodiesterase activity of MbaA either by enhancing or repressing the

inhibition dependent of the polyamine that is bound**.** Altering the phosphodiesterase activity of MbaA is thought to modify levels of c-di-GMP, affecting biofilm formation. The purpose of this study was to determine the potential binding surface on NspS that interacts with the periplasmic domain of MbaA. Utilizing a random mutagenesis approach and screening for mutant clones of interest, I identified 13 amino acids of NspS thought to be important to this interaction. A homology model of NspS was used to determine the location of the 13 residues allowing me to identify the region of NspS involved in the interaction with the periplasmic domain of MbaA. Based on the results of this study, I present a model of this periplasmic interaction in which NspS interacts with the periplasmic domain of MbaA to alter its phosphodiesterase activity and regulate biofilm formation in response to polyamines in the environment.

Acknowledgments

I would like to thank Dr. Darren Seals and Dr. Cort Bouldin for their willingness to serve on my committee as well as their helpful feedback and input to the progress of this work. I also want to express my deepest gratitude for my advisor, Dr. Ece Karatan, who was willing to take a chance on me. I have benefitted greatly from my time spent working in her lab and learning from her. I know that I am a better researcher and scientist because of the knowledge and experience she has so willingly shared.

There are many other faculty as well as graduate students that have contributed to this work in substantial ways. From helpful discussions to stress relief, the work presented in this thesis is better because of the community that exists in the Appalachian State Biology Department.

I would also like to acknowledge the Office of Student Research at Appalachian State for its support of this research via monetary funds for travel. This project was also supported by an NIH grant (number AI096358) from the National Institute of Allergy and Infectious Diseases awarded to Dr. Ece Karatan.

Dedication

I would like to dedicate this work to all of those who have supported me along the way. In particular, I'd like to thank my brother for his knowledge of all things in the world of biology and for enduring all of my questions about navigating that world. I'm also grateful to my parents for their endless belief that I can do whatever I set my mind to as well as my mom's constant willingness to serve as a grammar check throughout graduate school. Most especially, I dedicate this work to my husband without whom this would not have been possible.

Table of Contents

List of Tables

List of Figures

Foreword

This thesis will be submitted to *Microbiology*, an international peer reviewed journal published by the Microbiology Society. The organization and formatting of this thesis follow the requirements of the style guide for this journal.

Introduction

The human intestinal disease cholera affects millions of people worldwide and is responsible for thousands of deaths per year (1). The causative agent for cholera is the Gram-negative bacterium *Vibrio cholerae*, which resides as a natural inhabitant of many aquatic ecosystems including lakes, rivers, and oceans (2, 3). This bacterium can exist in two distinct states: a planktonic, free-swimming state or a sessile state that is associated with biofilm formation (4-6). The planktonic state is a highly motile state in which a flagellum is used for propulsion and virulence-related genes are highly expressed (7). The two main virulence factors of *V. cholerae* are toxin co-regulated pilus (TCP) and cholera toxin (CT) (8). TCP is a pilus that is required for the colonization of the small intestine and cholera toxin is an AB_5-subunit toxin in the ADP-ribosyltransferase family that is responsible for profuse watery diarrhea (8-10). In contrast to the motile, planktonic state, biofilms are aggregations or communities of cells surrounded by a matrix composed primarily of an extracellular polymeric substance (EPS) and can be found anchored to surfaces (11). The biofilm state provides a survival advantage to bacteria especially in harsh environments by providing increased resistance to antibiotics as well as protection against acidic pH and UV exposure (12-14). The proposed lifecycle for *V. cholerae* predicts that it exists primarily as a biofilm in aquatic environments, is ingested in part as a biofilm by humans to increase survival through the acidic conditions of the stomach, and then disperses from the biofilm once it reaches the small intestine to express virulence factors and cause disease (13, 15, 16).

This indicates the importance of regulating the transition between the planktonic and biofilm state for the lifecycle of this bacterium (13, 17).

The transition between these two states is regulated at the molecular level by the secondary messenger bis-(3'-5') cyclic dimeric guanosine monophosphate or c-di-GMP (18). C-di-GMP transcriptionally regulates the expression of genes encoding the proteins necessary for the synthesis of *Vibrio* polysaccharide and the other components that are crucial for construction of the biofilm matrix (18). Proteins with diguanylate cyclase (DGC) activity typically characterized by a GGDEF domain synthesize c-di-GMP from two molecules of GTP (19). Proteins with phosphodiesterase activity (PDE) break down c-di-GMP into either 5' pGpG or 2 molecules of guanosine monophosphate (GMP) (19). These proteins are typically characterized by either an EAL or HD-GYP domain (19). Each of these three c-di-GMP metabolic domains is named for the conserved amino acids important to its enzymatic function**.** Much of the current understanding about the regulation of biofilm formation involves the modulation of intracellular levels of c-di-GMP as it has been well established that high levels of c-di-GMP lead to increased biofilm formation, whereas low levels lead to a motile, planktonic lifestyle for *V. cholerae* (18-21).

Proteins that have GGDEF, EAL and/or HD-GYP domains tend to be a part of a larger protein that also contains sensory domains, likely to regulate the activity of these enzymatic domains based on signals received from the environment (11). One specific environmental signal regulating *V. cholerae* biofilm formation is polyamines. These molecules are aliphatic chains composed of two or more amine groups and positively charged at physiological pH that are synthesized by most organisms and are important for growth and cellular processes for most organisms (22, 23). The polyamines norspermidine,

spermidine, and spermine affect biofilm formation in *V. cholerae*; specifically, norspermidine enhances biofilm formation whereas spermidine and spermine inhibit it (24-27). Norspermidine is less prevalent than other polyamines and has been found in many species of *Vibrionaceae* and thermophilic bacteria as well as in eukaryotic algae, white shrimp, and arthropods (28-32). Spermidine and spermine are two of the most abundant polyamines present in the human intestine mostly due to dietary contributions or synthesis by intestinal cells; however, presence of the gut microbiota also adds to the level of spermidine found in the human intestine (33-35). The locations of these different polyamines and their effects on biofilm formation suggest a model in which *V. cholerae* can differentiate between the natural aquatic environment and the human intestine based on the presence of specific polyamines.

Polyamines that affect biofilm formation are processed by *V. cholerae* through a pathway composed of NspS, a periplasmic protein, and MbaA, a transmembrane protein with tandem cytoplasmic GGDEF and EAL domains (24-27). Previous studies have shown that NspS binds the polyamines norspermidine, spermidine, and spermine and the deletion of either *nspS* or *mbaA* abrogates the effects of polyamines on biofilm formation (24-27). Further**,** the EAL domain of MbaA has been characterized to have phosphodiesterase activity resulting in the breakdown of c-di-GMP (26, 36). The deletion of *mbaA* results in enhanced biofilm formation whereas the deletion of *nspS* results in an inhibition of biofilm formation, which suggests that NspS inhibits the PDE activity of MbaA (24). Thus, the current model for this signaling pathway is that NspS interacts with the periplasmic domain of MbaA to inhibit its PDE activity leading to an increase in c-di-GMP and an increase in biofilm formation (Figure 1) (24, 26). When NspS binds norspermidine, there is a greater inhibition

of the PDE activity of MbaA leading to enhanced biofilm formation presumably through increased levels of c-di-GMP (24, 26). In contrast, when NspS binds spermidine or spermine, the PDE activity is no longer inhibited resulting in the breakdown of c-di-GMP and a decrease in biofilm formation (25-27).

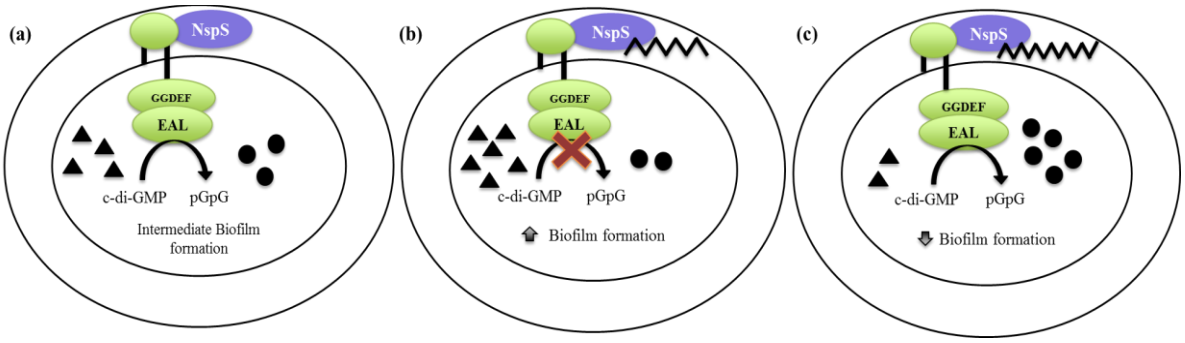

Fig 1. Model of NspS-MbaA signaling pathway. (a) Intermediate state of interaction in which NspS interacts with the periplasmic domain of MbaA to inhibit the PDE activity of MbaA and an intermediate amount of biofilm formation occurs. (b) When NspS is bound by norspermidine, there is a greater inhibition of the PDE activity of MbaA leading to higher levels of c-di-GMP and increased biofilm formation. (c) When NspS is bound by spermine (or spermidine), the inhibition of the PDE activity of MbaA is relieved resulting in c-di-GMP being broken down into pGpG and a decrease in biofilm formation. Black triangles represent c-di-GMP and black circles represent pGpG. The shorter zigzag line in (b) represents norspermidine and the longer zigzag line in (c) represents spermine. Adapted from (26, 27).

The aim of this study was to investigate the putative interaction between NspS and MbaA by identifying the amino acids of NspS important to the interaction with the periplasmic domain of MbaA. Through the introduction of random mutations into the *nspS* gene and subsequent screening, I identified the region of NspS thought to interact with the periplasmic domain of MbaA. Using the information determined from this study, I developed a working model of the periplasmic interaction between these two biofilm regulatory proteins.

Methods

Bacterial Strains and Growth Conditions

The strains in this study were derived from *Vibrio cholerae* O139 MO10. The bacterial strains and plasmids used in this study are listed in Table 1. *V. cholerae* strains were grown at 27°C and *E. coli* strains were grown at 37°C. All strains were grown in Luria-Bertani (LB) broth. Where appropriate, streptomycin was used at 100 μg mL^{-1}; tetracycline was used at 10 μg mL^{-1} for *E. coli* strains and at 2.5 μg mL^{-1} for *V. cholerae* strains. Primers were synthesized by Eurofins MWG Operon or Sigma and DNA sequencing was performed by Eurofins MWG Operon.

Table 1. Bacterial strains and plasmids.

Strain/Plasmid	Genotype	Source
Plasmids		
pACYC184	Cloning plasmid, Tet^R, Cm^R	New England Biolabs
pNP1	pACYC184::*nspS*-V5	(27)
***E. coli* strains**		
DH5α	F– Φ80*lacZ*ΔM15 Δ(*lac*ZYA-*arg*F) U169 *rec*A1 *end*A1 *hsd*R17 (rK–, mK+) *pho*A *sup*E44 λ– *thi*-1 *gyr*A96 *rel*A1	Invitrogen
AK006	DH5α with pACYC184	(37)
AK014	DH5α with pNP1	(37)
***V. cholerae* strains**		
PW249	MO10, clinical isolate of *V. cholerae* O139 from India, Sm^R	(38)

Table 1. (continued)

Strain/Plasmid	Genotype	Source
***V. cholerae* strains**		
PW514	MO10 *lacZ::vpsLp→lacZ, ΔnspS,* Sm^R	(24)
AK007	PW514 with pACYC184	(27)
AK831	PW514 with pNP1	(37)
AK944	PW514 with pACYC184::*nspS*-V5$_{R219S}$	This study
AK945	PW514 with pACYC184::*nspS*-V5$_{S216I}$	This study
AK946	PW514 with pACYC184::*nspS*-V5$_{S216R}$	This study
AK947	PW514 with pACYC184::*nspS*-V5$_{N268D}$	This study
AK948	PW514 with pACYC184::*nspS*-V5$_{S216N}$	This study
AK949	PW514 with pACYC184::*nspS*-V5$_{R219H}$	This study
AK950	PW514 with pACYC184::*nspS*-V5$_{F243V}$	This study
AK951	PW514 with pACYC184::*nspS*-V5$_{D263V}$	This study
AK952	PW514 with pACYC184::*nspS*-V5$_{V218L}$	This study
AK953	PW514 with pACYC184::*nspS*-V5$_{S79C}$	This study
AK954	PW514 with pACYC184::*nspS*-V5$_{L40H}$	This study
AK955	PW514 with pACYC184::*nspS*-V5$_{L89W}$	This study
AK956	PW514 with pACYC184::*nspS*-V5$_{L82R}$	This study
AK957	PW514 with pACYC184::*nspS*-V5$_{L82P}$	This study
AK958	PW514 with pACYC184::*nspS*-V5$_{S79G}$	This study
AK959	PW514 with pACYC184::*nspS*-V5$_{R219C}$	This study
AK960	PW514 with pACYC184::*nspS*-V5$_{N268S}$	This study
AK961	PW514 with pACYC184::*nspS*-V5$_{L40R}$	This study
AK962	PW514 with pACYC184::*nspS*-V5$_{F66V}$	This study
AK963	PW514 with pACYC184::*nspS*-V5$_{F84V}$	This study
AK964	PW514 with pACYC184::*nspS*-V5$_{D43N}$	This study
AK965	PW514 with pACYC184::*nspS*-V5$_{V218A}$	This study
AK966	PW514 with pACYC184::*nspS*-V5$_{L40P}$	This study
AK967	PW514 with pACYC184::*nspS*-V5$_{F66Y}$	This study

Error Prone PCR

Error prone PCR was performed on purified pNP1 plasmid using the GeneMorph II random mutagenesis kit (Agilent Technologies). Following manufacturer's instructions, 1 μg of target DNA was amplified for 30 cycles to achieve an approximate mutational frequency of 0-4.5 mutation(s) per kilobase. The cycling conditions were as follows: initial denaturation at 95°C for 2 minutes, 30 cycles of denaturation at 95°C for 30 seconds, annealing at 53°C for 30 seconds, and extension at 72°C for 1.5 minutes, and a final extension at 72°C for 10 minutes.

***nspS* Mutant Library Generation**

Gel purified products from the error prone PCR reaction and purified pACYC184 plasmid were digested with restriction enzymes *Nco*I and *Eco*RI. The PCR products were ligated into pACYC184 using ElectroLigase following manufacturer's recommendations (New England Biolabs). After ligation, the plasmid products were transformed into *E. coli* DH5α. Successful transformation was confirmed by PCR and sequencing using the forward primer P291 (5' GCATGATGAACCTGAATCGC), which anneals upstream of the *Nco*I digest site used for cloning into pACYC184, and the reverse primer P292 (5' GCCTTTATTCACATTCTTGCC), which anneals downstream of the *Eco*RI digest site used for cloning into pACYC184. To generate the final mutant library, the ligated pACYC184::mutant-*nspS*-V5 plasmid was transformed again into DH5α. One mL LB was added to each agar plate on which there was growth post-transformation and the colonies were scraped using a plate spreader so they were resuspended into the LB. The LB from each plate was combined and a midi prep was performed with a Wizard Plus Midiprep DNA

purification kit (Promega) to purify the plasmids. This process was repeated a second time to generate the final *nspS* mutant library.

Screening for Biofilm-deficient Mutants

Following transformation of the final *nspS* mutant library into a Δ*nspS* strain of *V. cholerae,* individual colonies were inoculated in LB with appropriate antibiotics into separate wells of a 2 mL 96-well plate and grown overnight shaking at 27°C. The following day, the overnight culture was diluted 1:50 in fresh media in new wells of 2-mL 96-well plate shaking at 27°C until the bacteria reached mid-log phase. Each well was diluted to an OD_{655} of 0.04 in 125 µl in 96-well microtiter plates and these plates were grown statically at 27°C for approximately 24 hours. They were then assessed for biofilm formation using a modified version of the crystal violet biofilm staining protocol described previously (39). Briefly, planktonic cells were removed and the remaining biofilm washed with 1X phosphate buffered saline (PBS). A 1% crystal violet solution was used to stain the biofilm for 25 minutes. After removal of the stain, two consecutive 1X PBS wash steps were performed. The microtiter plates were dried and the crystal violet was solubilized in 135 µl of 95% ethanol for approximately 10 minutes. The absorbance of 125 µl from each well was analyzed at a wavelength of 595 nm. After the initial transformation of the *nspS* mutant library, biofilm formation was analyzed in triplicate for one biological replicate of each mutant clone. Based on these results, mutant clones that were different from the positive control, *V. cholerae* Δ*nspS* with pACYC184::*nspS,* were analyzed again for biofilm formation using the same protocol described above. For the second biofilm assay using

crystal violet staining, three biological replicates were assessed in triplicate for each "down" mutant clone to confirm the low biofilm phenotype seen in the initial screen.

Western Blot Analysis

Following overnight growth at 27°C shaking, cells were pelleted by centrifugation, resuspended in 250-300 µl 1X PBS, sonicated 3 times for 10 seconds each, and centrifuged at 16,000 x g for 20 minutes at 4°C. The supernatant was combined with Laemmli sample buffer containing β-mercaptoethanol in a 1:1 ratio and incubated at 65°C for 5 minutes. Each sample was run on a polyacrylamide gel for between 1 to 1.5 hours at 240 V. The gel was transferred onto a PVDF membrane using a BIO-RAD Mini Trans Blot for between 45-70 minutes. After the transfer, the membrane was blocked for either 1 hour at room temperature or 4 hours at 4°C in 5% (w/v) non-fat dry milk in 1X PBS-T (0.05% (v/v) Tween 20 solution in 1X PBS) after which it was washed 3 times for 5 minutes with 1X PBS-T. The membrane was then incubated for 1 hour at room temperature with mouse monoclonal anti-V5 Tag antibody conjugated with Horseradish Peroxidase (HRP) (BIO-RAD) diluted 1:5000 and a Precision Protein StrepTactin-HRP Conjugate antibody (BIO-RAD) diluted 1:10,000. The anti-V5 antibody was utilized to react with the V5 tag that was engineered into the *nspS* sequence when it was cloned into pACYC184. The membrane was washed 3 times for 5 minutes with 1X PBS-T and was then incubated with SuperSignal West Pico Chemiluminescent Substrate (Thermo Scientific) for 5 minutes. The membrane was imaged with a BIO-RAD Molecular Imager Gel Doc XR System.

Biofilm Assay

Overnight cultures were diluted 1:50 into 2 mL new LB media with antibiotics and grown to mid-log phase shaking at 27°C. Strains were diluted to an OD_{655} of 0.04 in 0.3 mL LB with antibiotics in borosilicate test tubes in the absence or presence of norspermidine. These tubes were incubated statically at 27°C for 24 hours. After incubation, planktonic cells were removed and the remaining biofilm was washed with 0.3 mL 1X PBS. The biofilm was homogenized by vortexing for 30 seconds with 1.0 mm glass beads (BioSpec) in 0.3 mL 1X PBS. The cell density of the homogenized biofilm was measured at OD_{655} using an iMark Microplate Reader (BIO-RAD). All experiments were performed in triplicate and repeated for reproducibility.

Sequencing and Analysis

Plasmids were isolated from mutant clones of interest and sent for sequencing using the forward primer P291 and the reverse primer P292. Primers P37 (5' CGTTTTGGCTAACGTCTCCGCG) and P39 (5' GGTATGCTTAAAGCCAGTGTCG) were utilized when necessary for additional sequencing. These primers anneal to nucleotides 261-282 and nucleotides 496-517 of the *nspS* gene respectively. The sequencing results were analyzed using Vector NTI (Thermo Scientific). A contig was generated for each sequenced mutant clone and was translated into a protein sequence for alignment against the wild type NspS protein sequence to determine changes in amino acids.

Bioinformatics

The intensive mode of the Phyre2 web portal for protein modeling, prediction, and analysis (http://www.sbg.bio.ic.ac.uk/servers/phyre2/html/page.cgi?id=index) was used to generate a homology model of the NspS protein using an input of six different proteins as templates: PotF, a putrescine receptor in *E. coli;* PotD, a spermidine and putrescine binding protein in *Streptococcus pneumoniae*; SpuD and SpuE, polyamine binding proteins in *Pseudomonas aeruginosa*; an unnamed putative spermidine and putrescine ABC transporter in *Listeria monocytogenes*, and PotD spermidine and putrescine binding protein in *E. coli* (40). The UCSF ChimeraX molecular visualization program was utilized to manipulate and generate images of the NspS homology model (41). A CLUSTALW multiple sequence alignment was performed for NspS and five identified homologs from other bacterial species (26, 42, 43). These five NspS-like proteins are Ping_1238 from *Psychromonas ingrahamii* (NCBI Accession number: WP_011769631), HCH_06688 from *Hahella chejuensis* (NCBI Accession number: WP_011400370), Ssed_2394 from *Shewanella sediminis* (NCBI Accession number: WP_012142738), PST_0371 from *Pseudomonas stutzeri* (NCBI Accession number: WP_011911609) and SMc_00991 from *Sinorhizobium meliloti* (NCBI Accession number: NP_384966). The output from this alignment was visualized and a final image generated with ESPript 3.0 (44).

Results

Construction of a *nspS* Mutant Library

To introduce random mutations, the wild type *nspS* gene was subjected to error prone PCR. Following purification, the error prone PCR products were cloned into the plasmid pACYC184 and transformed into DH5α *E. coli* cells. Based on a small subset of mutant clones that were sequenced, the mutation rate was determined to be approximately 50% and the missense mutation rate was estimated to be approximately 30% (data not shown). This confirmed the success of the error prone PCR. Two subsequent rounds of transformation of pACYC184::mutant-*nspS*-V5 into DH5α yielded a final mutant library size estimated by colony count to be composed of approximately 20,000 mutant clones.

Screening of mutant clones for low biofilm formation and NspS protein expression

Following the successful construction of the final *nspS* mutant library, the development of a screening process to identify mutant clones of interest was necessary. A *nspS* deletion strain of *V. cholerae* forms a low amount of biofilm (24) presumably because NspS can't interact with the periplasmic domain of MbaA to inhibit the phosphodiesterase activity of the EAL domain. Based on this premise, mutations in the amino acids of NspS important to the interaction with the periplasmic domain of MbaA should also result in strains with low biofilm formation. Thus, a high-throughput screening method (Figure 2) was developed in which crystal violet staining was utilized to assess the amount of biofilm formation for mutant clones in the *nspS* mutant library.

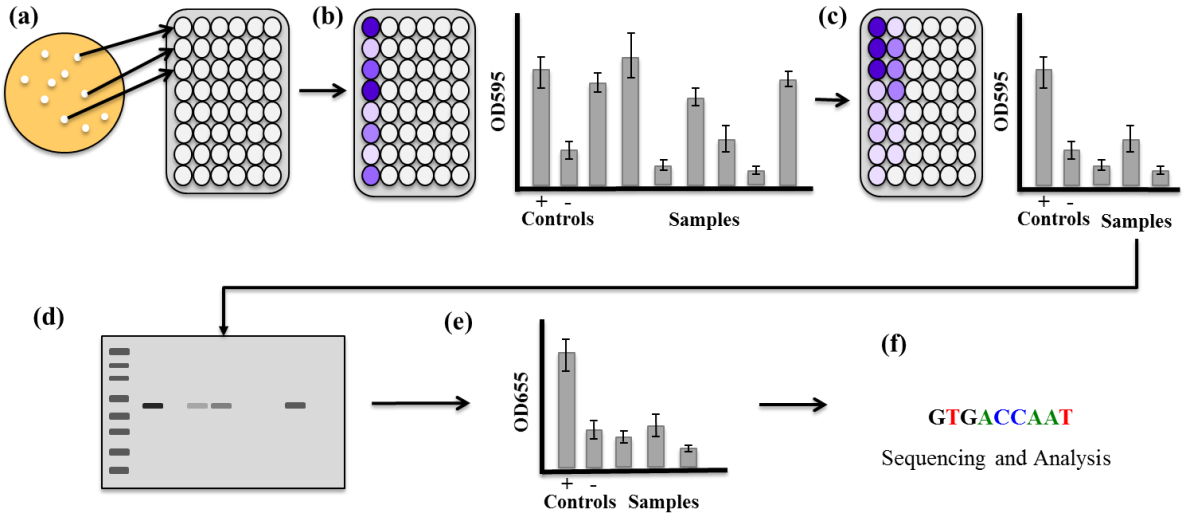

Fig 2. Mutant Clone Screening Process. (a) The *nspS* mutant library was transformed into *V. cholerae* Δ*nspS* strain and colonies were individually grown in separate wells of a 96-well deepwell plate. (b) For each mutant clone, crystal violet staining was performed to assess biofilm formation for one biological replicate. (c) Biofilm formation using crystal violet stain was used again to assess three biological replicates for mutant clones with low biofilm formation in the initial assay. (d) Mutant clones that produced low biofilms were analyzed via western blot for protein expression. (e) For clones that had protein expression, a final biofilm assay was performed that measured the cellular density of the biofilm to confirm the low biofilm phenotype. (f) Any mutant clones that had low biofilm formation and protein expression that was detected via western blot were purified and sent for sequencing and analysis.

After transformation of the *nspS* mutant library into a *V. cholerae* Δ*nspS* strain, biofilm formation was analyzed in triplicate for one biological replicate of each mutant clone. In total, 1,441 mutant clones were screened for biofilm formation with this initial crystal violet staining biofilm assay. As expected, there was a large amount of variation in biofilm formation between different mutant clones during this initial assay as seen in an example biofilm graph of 96 mutant clones in Figure 3. Based on these results, only mutant clones that were different from the positive control, *V. cholerae* Δ*nspS* with pACYC184::*nspS*, were analyzed again for biofilm formation. For the second biofilm assay using crystal violet staining, three biological replicates were assessed in triplicate each for each "down" mutant

clone to confirm the low biofilm phenotype seen in the initial screen. Of the 1,441 mutant clones screened, 338 were determined to be "down" mutant clones due to low biofilm formation and were analyzed again with a second assay for biofilm formation using crystal violet staining.

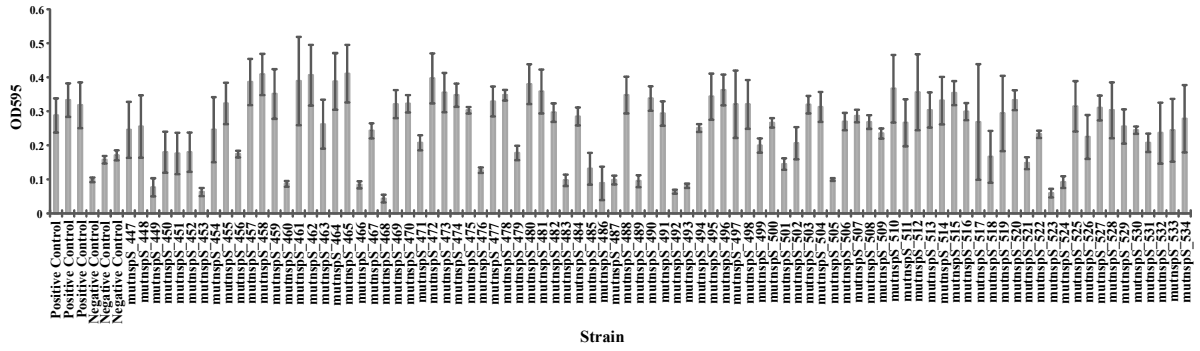

Fig 3. Initial biofilm analysis for a set of 96 mutant clones. Crystal violet staining was used to analyze biofilm formation for each mutant clone. The positive control is *V. cholerae* Δ*nspS* with pACYC184::*nspS*-V5 and the negative control is *V. cholerae* Δ*nspS* with pACYC184. The error bars represent standard deviations of three technical replicates.

After the second step in the screening process, the 293 mutant clones confirmed to have a low biofilm phenotype were analyzed for NspS protein expression. This was accomplished with western blots by probing with a monoclonal anti-V5 tag antibody that recognized the V5 tag engineered to the C-terminus of NspS. Mutant clones showing protein expression at the correct size as the positive control, approximately 40 kDa, were continued forward in the screening process. Of the 293 mutant clones analyzed, there were 106 that had V5 expression indicating the presence of the NspS protein. In an example western blot of seven mutant clones (Figure 4a), only mutnspS_426, mutnspS_456, mutnspS_486 and mutnspS_487 showed NspS protein expression and were continued forward in the process for further analysis. Any mutant clones for which protein expression could not be detected on a

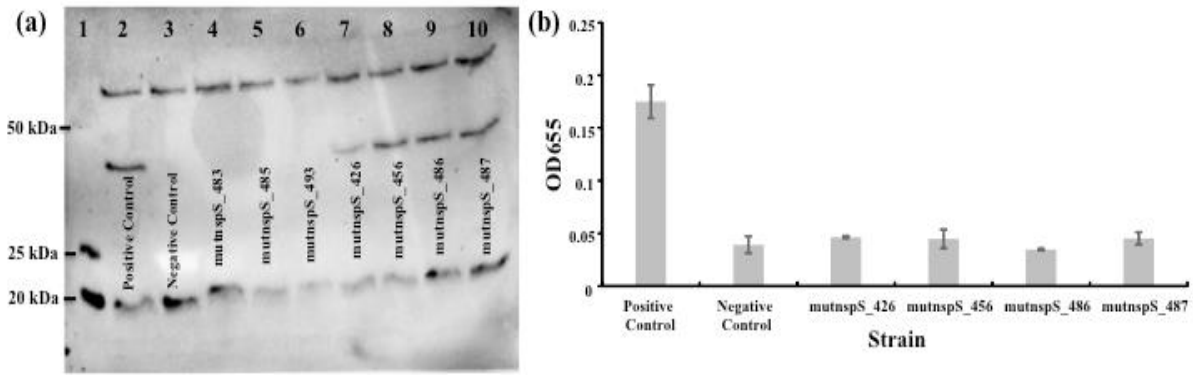

Fig 4. Analysis of NspS protein expression and tertiary screen of biofilm formation. (a) Western blot analysis with a ladder in Lane 1 and positive and negative controls respectively in Lanes 2 and 3. The positive control is *V. cholerae* Δ*nspS* with pACYC184::*nspS*-V5 and the negative control is *V. cholerae* Δ*nspS* with pACYC184. Lanes 4-10, seven mutant clones identified from two crystal violet biofilm assays as having low biofilm formation. This image was taken with a BIO-RAD Molecular Imager Gel Doc XR System and manually exposed for two minutes. (b) Graph of biofilm formation for the four mutant clones from (a) that showed NspS protein expression. Three biological replicates were analyzed in triplicate per mutant clone for biofilm formation. The positive and negative controls are the same as in (a). Error bars show standard deviations of three biological replicates.

western blot were assumed to either have mutations that prevented proper folding and therefore did not result in stable protein or had mutations that resulted in truncated proteins through the introduction of premature stop codons. In either case, these mutants were not of interest to the study and were not investigated further.

The last step in the screening process was a final assessment of mutant clone biofilm formation using a different method than crystal violet staining to confirm the low biofilm phenotype. Mutant clones that showed NspS expression were analyzed for biofilm formation by homogenizing the biofilm with glass beads and measuring the cell density. Figure 4b is an example graph of this assessment showing the cell density of the biofilms for the four mutant clones in Figure 4a that had NspS protein expression as well as the biofilm cell density of the positive and negative controls for comparison. All of the 106 mutant clones

that showed NspS protein expression were assessed for biofilm formation for a third time. Ninety-eight mutant clones still showed a low amount of biofilm formation in this final assay. Plasmids were isolated from these mutant clones and the sequence of the cloned *nspS* gene was determined.

Amino acids identified in the mutant clone screen

Of the 1,441 mutant clones initially screened, 73 mutant clones were successfully sequenced and changes from the wild-type NspS sequence were determined (Table 2a-c). There were 43 clones with one missense mutation, 24 with two, five with three and one with four missense mutations.

Table 2. Mutations identified in sequenced mutant clones. (a) Mutant clones with single missense mutations (b) Mutant clones with double missense mutations (c) Mutant clones with either three or four missense mutations. All mutations are listed as the wild type amino acid, the position of the amino acid followed by the amino acid mutation determined from sequencing.

(a)

Single Missense Mutations:			
Mutant Clone	**Mutation Identified**	**Mutant Clone**	**Mutation Identified**
mutnspS_69	F84V	mutnspS_686	L89W
mutnspS_85	R219S	mutnspS_724	N68I
mutnspS_148	S216I	mutnspS_732	R219H
mutnspS_205	R219C	mutnspS_797	R242L
mutnspS_221	S216R	mutnspS_853	L82P
mutnspS_255	N268D	mutnspS_921	S79G
mutnspS_260	N268D	mutnspS_934	D43N
mutnspS_261	S79G	mutnspS_963	F243V
mutnspS_264	S216N	mutnspS_1047	R219C
mutnspS_273	S216R	mutnspS_1084	S216N
mutnspS_387	R219H	mutnspS_1089	N268S
mutnspS_415	F243V	mutnspS_1095	L40R
mutnspS_426	D263V	mutnspS_1147	F66V
mutnspS_430	S32N	mutnspS_1155	F84V
mutnspS_456	V218L	mutnspS_1233	F64L
mutnspS_568	D263V	mutnspS_1239	S79C
mutnspS_573	P83L	mutnspS_1255	D43N
mutnspS_580	S79C	mutnspS_1261	V218A
mutnspS_585	L40H	mutnspS_1327	L40P
mutnspS_605	L89W	mutnspS_1371	F66Y
mutnspS_675	L82R	mutnspS_1390	L281F
mutnspS_684	L82R		

(b)

Double Missense Mutations:	
Mutant Clone	**Mutations Identified**
mutnspS_3	L75F, S171N
mutnspS_25	W8R, Y213N
mutnspS_212	N62I, D263N
mutnspS_233	S79G, S216G
mutnspS_246	S79G, S216G
mutnspS_320	V80I, D263E
mutnspS_453	P117H, S216N
mutnspS_468	S79G, S216G
mutnspS_486	F84V, T149A
mutnspS_558	R219C, D236V
mutnspS_629	D69V, R219L
mutnspS_652	N68I, A94T
mutnspS_693	N68I, A94T
mutnspS_707	S79N, L182H
mutnspS_719	M14K, S79G
mutnspS_731	L82V, A108S
mutnspS_844	P117H, S216N
mutnspS_867	S79R, N268I
mutnspS_907	H126Y, S216N
mutnspS_1202	A33D, N115K
mutnspS_1222	A33D, N115K
mutnspS_1294	S79N, P117S
mutnspS_1355	R112P, D236E
mutnspS_1384	D67N, L341H

(c)

Multiple Missense Mutations:	
Mutant Clone	**Mutations Identified**
mutnspS_118	D170Y, N183H, F283I
mutnspS_1104	R112H, P177H, L343P
mutnspS_1279	S79G, I187N, S337L
mutnspS_1308	S216G, K286I, E295V
mutnspS_1423	E42G, V102I, E173K
mutnspS_294	P83H, K146E, S220N, P311L

The single missense mutations were given the focus of investigation for the remainder of this study as more than one mutation presents the difficulty of having to parse out the effects of each individual mutation. Of the 43 single missense mutations that were identified by the screen, there were only 19 unique amino acids of NspS affected. Thirteen of these occurred in more than one mutant clone providing additional support that these amino acids could be important to the interaction between NspS and the periplasmic domain of MbaA.

For some of these 13 amino acids, the mutation was the same change (i.e. phenylalanine at position 243 was mutated twice, both times to a valine); however, in other cases, there were multiple different changes that occurred. This was true for the arginine at position 219, which was mutated to a cysteine, a histidine, and a serine in different mutant clones. Interestingly, some of the amino acids that occurred as single mutations also appeared as one of the mutations in clones with double missense mutations. In particular, asparagine 68, serine 79, serine 216, arginine 219, and aspartic acid 263 all occurred more than once in a clone with a double missense mutation. The frequency at which these residues were identified by the screening process suggested that further investigation into the effects of these mutations was warranted.

Norspermidine addition had a varying effect on NspS mutant clone biofilm formation

Previous work has demonstrated that NspS binds the polyamines spermine, spermidine, and norspermidine (24, 26, 27). Spermine and spermidine inhibit biofilm formation in *V. cholerae*. Since the mutant clones of interest have already been shown to form low biofilms, it would be very difficult to detect a response to either one of these polyamines. In contrast, norspermidine enhances biofilm formation presumably through the function of NspS as deletion of *nspS* abrogates the effect of norspermidine (24). To test the effect of norspermidine on the single mutations of NspS identified by the screen, biofilm formation for each mutant clone was analyzed in the absence of and presence of 100 μM exogenous norspermidine (Figure 5).

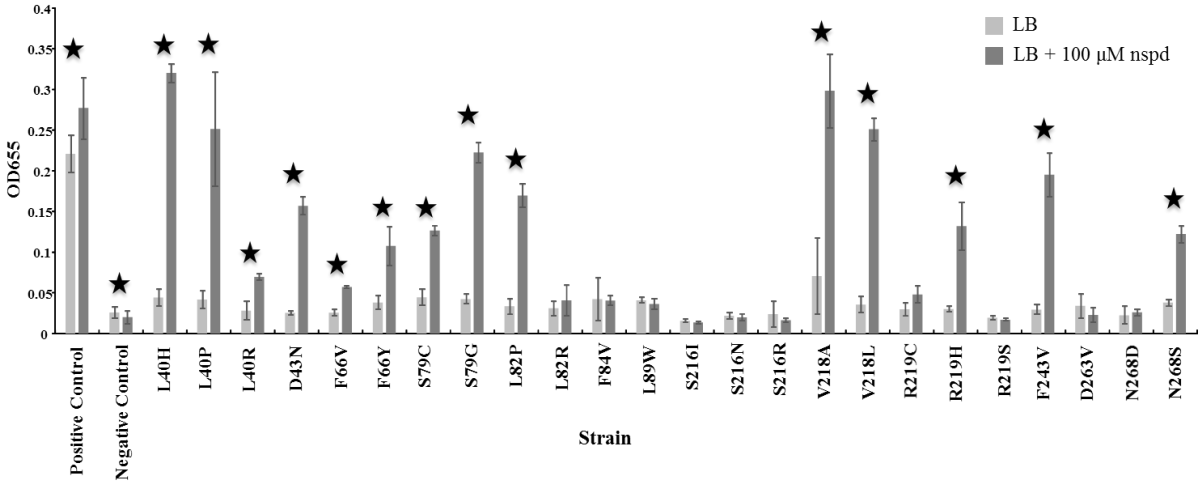

Fig 5. Effects on biofilm formation of single missense NspS mutant clones with or without exogenous norspermidine. The experiments were performed in triplicate and the error bars show the standard deviation of three biological replicates. Each mutant clone is listed only by the single missense mutation present in that strain of *V. cholerae* Δ*nspS* pACYC184::*nspS*-V5. The positive control is *V. cholerae* Δ*nspS* pACYC184::*nspS*-V5 and the negative control is *V. cholerae* Δ*nspS* pACYC184. A t-test was used to compare biofilm formation between LB only and LB + 100 µM nspd for each individual mutant clone analyzed. A star indicates a statistically significant difference in biofilm formation with and without the addition of norspermidine. A p-value of <0.05 was considered significant.

In response to the addition of norspermidine, some of the mutant clones were unresponsive, some were desensitized, and some responded with biofilm formation that was similar to that of the positive control (Table 3). About half of the mutant clones analyzed did have a statistically significant increase in biofilm formation when exogenous norspermidine was added to the LB. Those mutant clones that did have an increase in biofilm formation were denoted as either desensitized or responsive to the norspermidine based on the amount of biofilm formation. The mutant clones that did not have a significant increase in biofilm formation were considered to be unresponsive. Interestingly, mutant clones with a mutation in the serine 216 were unresponsive to norspermidine addition regardless of the type of the amino acid change. This was not the case for other mutant clones such as arginine 219, which showed a significant increase in biofilm formation in the presence of 100 µM when

changed to a histidine, but not when changed to a cysteine or serine. These results might provide insight into amino acids that may contribute to the mechanism by which NspS binds norspermidine.

Table 3. Categorization of mutant clone response to exogenous norspermidine. Each mutant clone is listed only by the single missense mutation present in that strain of *V. cholerae* Δ*nspS* pACYC184::*nspS*-V5.

Unresponsive Mutant Clones	Desensitized Mutant Clones	Responsive Mutant Clones
L82R, F84V, L89W, S216I, S216N, S216R, R219C, R219S, D263V, N268D	L40R, D43N, F66V, F66Y, S79C, S79G, L82P, R219H, F243V, N268S	L40H, L40P, V218A, V218L

Mutations identified in the screening process cluster in two distinct locations on NspS

Previous research has demonstrated that even though NspS can bind polyamines, it does not play a role in transport (26); however, the closest homologs to NspS whose structures have been determined are polyamine transport proteins. To determine the location of the mutated amino acids identified by the screening process, six of these proteins were used as templates to construct a NspS homology model using Phyre2 (40). Using the ChimeraX program (41), a ribbon model diagram was generated and the 13 amino acids that occurred in more than one missense mutation mutant clone were highlighted with a pink color and space fill option (Figures 6a and 6b). The amino acids were determined to be in two main groups or locations on the homology model (Figure 6b). Further analysis of the homology model revealed that the highlighted amino acids appeared as though they might be on or close to the surface of NspS.

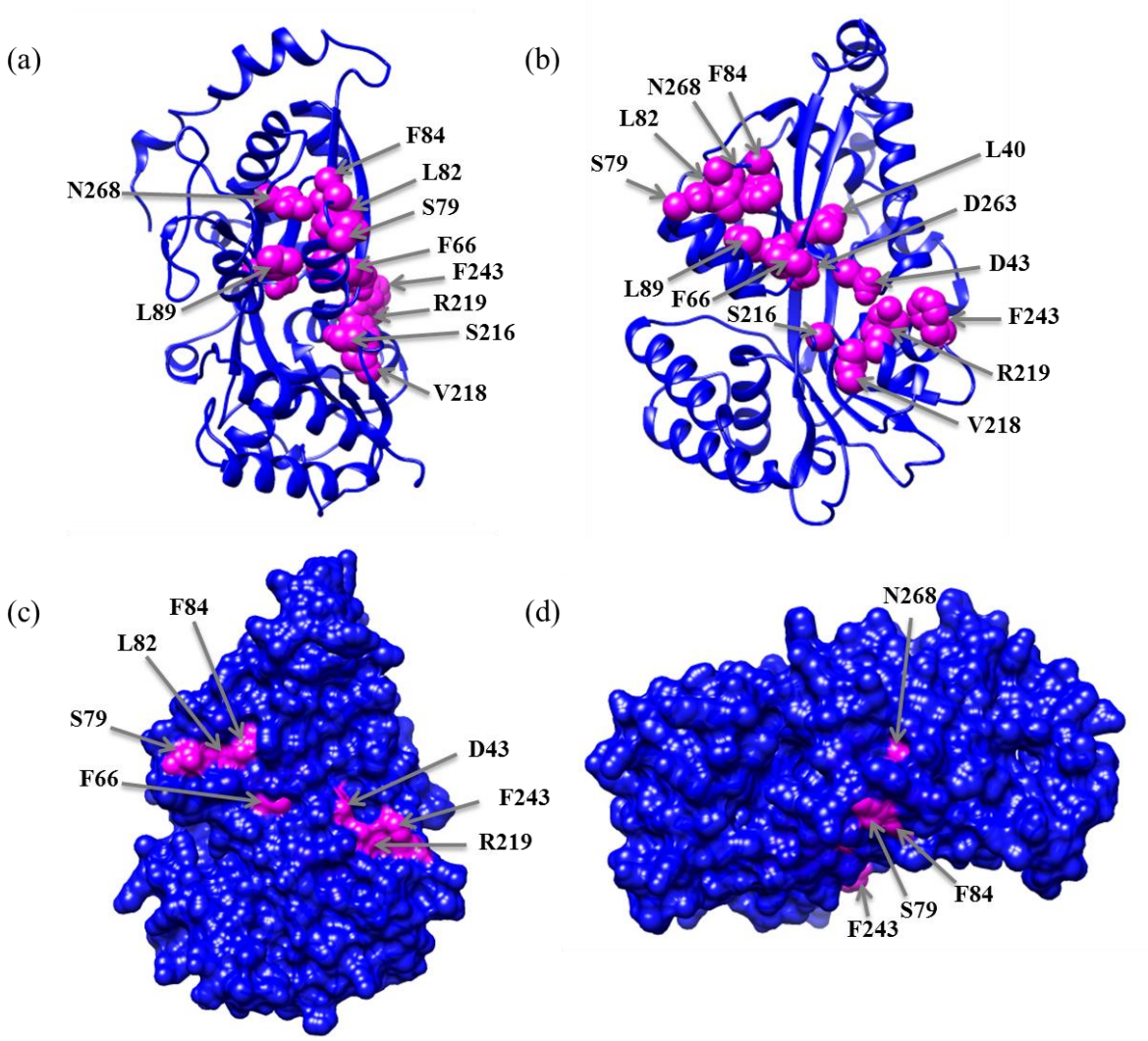

Fig 6. NpsS homology model. (a) Ribbon-diagram model of NspS with a side view of the protein. (b) Same as (a) but view has been rotated to look at a "center" view into the mouth of the protein. (c) Same as (b) but with the surface filled in/added to the homology model. (d) Same as (c) but rotated down to demonstrate a different view/angle of NspS.

In order to investigate this possibility, the surface of the protein was added to the homology model. The pink color of several of the highlighted amino acids was apparent when viewing the homology model (Figure 6c). This indicates that these amino acids are likely on the surface of NspS, which may provide one continuous surface or multiple points of interaction with the periplasmic domain of MbaA. To examine the possibility of how the point(s) of interaction may interact with MbaA, the homology model was adjusted to

different angles. One specific view (Figure 6d) revealed a groove that could provide a surface of interaction with another protein. The location of the mutated amino acids identified in the screening process provided further support for this hypothesis.

Conserved amino acids of NspS were identified from protein alignment

Previous work has identified other NspS/MbaA pairs of proteins present in other *Proteobacteria* (26). Five NspS-like proteins with predicted polyamine ligands were utilized to generate a protein alignment against NspS to determine conserved amino acids (Figure 7). The alignment showed that 22 different amino acid positions were conserved across all six proteins. There were also many other cases in which positions had a consensus residue, meaning that greater than 50% of the proteins had the same amino acid at that position. Further, a short sequence of amino acids from approximately position 126 to position 144 was identified that appeared to be the most well conserved area among these six proteins. Interestingly, the only mutation in this 18-residue stretch that occurred in the screening process was a mutant clone with a double missense mutation in which one of the mutations was a change from histidine at position 126 to tyrosine. As seen in the alignment, NspS has a histidine at that position, whereas four of the homologs have a tyrosine indicating that this mutation may not have a significant impact on the structure of NspS. The lack of mutations identified in this area of the NspS protein may suggest that the conservation seen in this 18-bp amino acid stretch may be so integral to its protein structure that those residues cannot be altered without a detrimental effect on its structure.

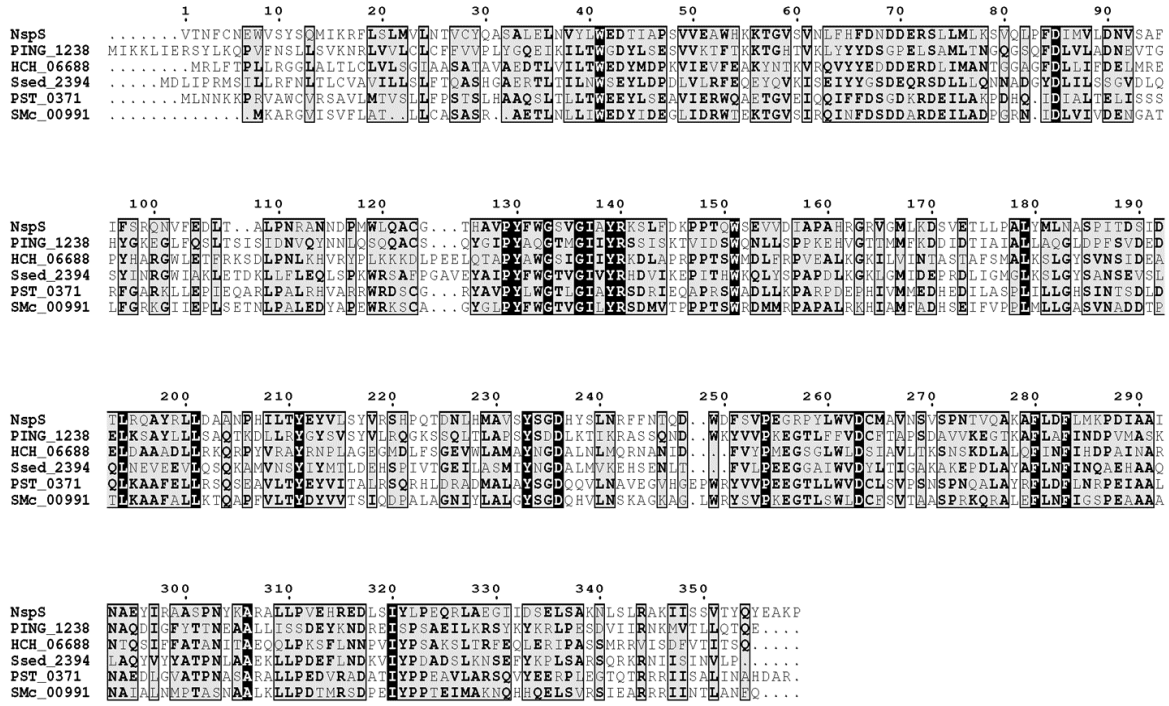

Fig 7. Protein alignment comparing NspS sequence to five NspS-like proteins identified in other bacterial species. Each protein in this alignment has one or more polyamines as its predicted ligand. Clustal W alignment software was used to compare these six proteins and the final image was generated using ESPript 3.0 (42-44). The positions in the alignment highlighted in black indicate one identical amino acid across all six proteins. The positions highlighted in gray indicate some similarity across the six proteins and is indicated in boldface font. Numbered positions are based on the NspS protein sequence.

When the 13 amino acids that were mutated in more than one mutant clone were examined on the protein alignment, there was only one conserved across all six proteins, the aspartic acid at position 263**.** In another case, the aspartic acid at position 43 of NspS was also mutated in multiple mutant clones. The protein alignment in Figure 7 shows that three of the NspS-like proteins have an aspartic acid at this position while the other two have a glutamic acid. This indicates the conservation of an amino acid with a negatively charged side chain at this position for these proteins. At position 66, half of the proteins, including NspS, have a phenylalanine and the other half have a tyrosine. This indicates the importance

of a non-polar aromatic amino acid at this position for these proteins. There are several amino acids of the 13 that do not have similarity across these six proteins; however, some of them are located near well conserved amino acids. For example, both leucine 40 and aspartic acid 43 are in close in proximity to the tryptophan conserved across all six proteins at position 41. Also, serine 79, leucine 82, phenylalanine 84, and leucine 89 are all clustered near an aspartic acid residue at position 85 that is identical for all six proteins. This suggests the possibility that amino acids 41 and 85 could be important to the interaction between NspS and the periplasmic domain of MbaA. While our screening process did not show mutations in these specific residues, it remains possible that mutations in residues in close proximity disrupted the binding interface of NspS to affect interaction.

Discussion

Vibrio cholerae biofilm formation is regulated by specific polyamines in the environment including spermine, spermidine, and norspermidine. Based on previous research, the proposed model for the signal transduction of polyamines occurs through a pathway composed of NspS, a periplasmic binding protein, and MbaA, a transmembrane protein with tandem cytoplasmic GGDEF and EAL domains (24-27). The interaction of NspS with the periplasmic domain of MbaA is proposed to alter the phophodiesterase activity of the EAL domain of MbaA, which presumably affects the intracellular level of the secondary messenger c-di-GMP. This study aimed to identify the amino acids of NspS important to the interaction with the periplasmic domain of MbaA to elucidate more information about the mechanism of this signal transduction.

In this study, we utilized a mutagenic screen to identify amino acids of NspS important to the interaction with the periplasmic domain of MbaA. This screening process yielded 13 amino acids thought to be involved in this interaction. Analysis of biofilm formation of the mutant clones identified in this study after the addition of norspermidine confirmed a role for these residues in the signal transduction of norspermidine. Certain mutations abrogated the effect of norspermidine indicating that without a specific amino acid in certain positions, NspS cannot interact properly with the periplasmic domain of MbaA to inactivate its phosphodiesterase activity. Interestingly, other identified amino acids did not

appear to have the same effect indicating that they may only play a contributory role or the change in amino acid was not significant enough from the wild type to affect the interaction.

Locating the 13 amino acids on the NspS homology model led to the hypothesis that these amino acids could either form one continuous surface of interaction or two distinct points of contact with the periplasmic domain of MbaA. The homology model was rotated to an angle that presented a groove for binding to another protein (Figure 8a). Combined with the location of the amino acids and the presence of a groove, this suggests that NspS sits on top of the periplasmic domain of MbaA relative to the inner membrane (Figure 8b). The predicted pocket for polyamine binding is unobstructed in this orientation and could provide the mechanism by which conformation changes occur that are then relayed to the cytoplasmic domains of MbaA.

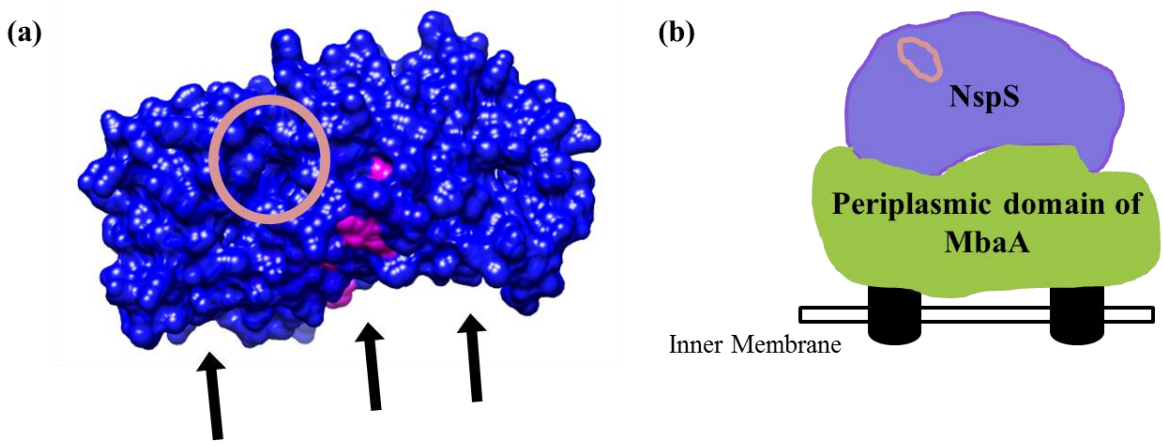

Fig 8. Proposed model of interaction between NspS and the periplasmic domain of MbaA. (a) Surface-filled Homology Model of NspS. The pink amino acids were identified by the mutagenesis screen. The orange circle highlights the predicted ligand binding pocket where polyamines would bind and the black arrows point to the potential point of interaction with the periplasmic domain of MbaA. (b) Cartoon model of the interaction between NspS and MbaA relative to the inner membrane. The orange oval on NspS represents the predicted ligand binding pocket where polyamines would bind.

Based on the NspS/MbaA signal transduction pathway model, there are three different states of interaction between these two proteins (26). Low biofilm formation in presence of the polyamines spermine or spermidine, an intermediate amount of biofilm formation when no polyamines are bound by NspS, and high biofilm formation when norspermidine is present in the environment. Three proposed states of interaction suggest that NspS and the periplasmic domain of MbaA interact constitutively and a conformational change occurs to alter the PDE activity of MbaA only when NspS is bound to a polyamine. The idea of this constitutive interaction is supported in literature by other examples of periplasmic binding proteins (PBPs) interacting with transmembrane proteins. An example of this is the two-component system in *Vibrio harveyii* that responds to quorum sensing signals to generate bioluminescence. In this pathway, LuxP is a PBP that constantly interacts with LuxQ, a sensor kinase spanning the inner membrane; however, when LuxP binds to its ligand, autoinducer-2, this alters the conformation of LuxQ and results in the inactivation of the kinase activity of its intracellular domain (45). The data from our study supports this model of the pathway in which NspS and the periplasmic domain of MbaA are constitutively interacting and conformational changes occur when polyamines bind to NspS.

We acknowledge that there are shortcomings in relying on a homology model of NspS based on the structure of other proteins. Given the difficulties and the labor-intensive process involved in the crystallization of a protein, a homology model of NspS can nevertheless be helpful. It was intentional that multiple template proteins were utilized rather than just one as a way to increase the accuracy of the NspS homology model. However, moving forward, working towards solving the structure of NspS would ultimately enable

better study of this system. The results from this study would be able to then be tested or examined on a structure known to be accurate. Further, we have also not discounted the possibility that the stoichiometry of this interaction may not be 1:1 and that dimerization of one or both proteins may be important to this interaction. There are other examples of periplasmic binding proteins in which a periplasmic protein as a monomer interacts with a dimer of a transmembrane protein such as a pathway in *P. fluorescens* that regulates biofilm formation in response to levels of inorganic phosphate (46). In this case, the transmembrane protein LapD must dimerize to form the binding site required for the periplasmic LapG protein. Further work investigating this possibility for my own signaling pathway will be required before a complete picture of the proposed NspS-MbaA interaction is elucidated. The results from this study support the hypothesis that NspS and the periplasmic domain of MbaA interact to transduce polyamines in the environment as well as provide a model depicting that interaction.

This mechanism demonstrates a signaling paradigm in which bacterial species are able to differentially sense signals in the environment, transduce the information into the cell and modify their behavior to respond accordingly. With the identification of multiple homologous NspS/MbaA pairs in other *Proteobacteria* (26), understanding this signaling system could not only elucidate information about how *V. cholerae* interacts with its environment but also how other bacterial species do as well.

References

1. **Ali M, Nelson AR, Lopez AL, Sack DA**. Updated global burden of cholera in endemic countries. *PLoS Negl Trop Dis*. 2015;9(6):e0003832.

2. **Kierek K, Watnick PI**. Environmental determinants of *Vibrio cholerae* biofilm development. *Appl Environ Microbiol*. 2003;69(9):5079-88.

3. **Colwell RR, Spira WM**. The Ecology of *Vibrio cholerae*. In: Barua D, Greenough WB, editors. Cholera. Current Topics in Infectious Disease. Boston, MA: Springer; 1992. p. 107-27.

4. **Faruque SM BK, Udden SM, Ahmad, QS, Sack DA, Nair GB, Mekalanos, JJ**. . Transmissibility of cholera: in vivo-formed biofilms and their relationship to infectivity and persistence in the environment. *Proc Natl Acad Sci U S A*. 2006;103(16):6350-5.

5. **Richardson K**. Roles of motility and flagellar structure in pathogenicity of *Vibrio cholerae*: analysis of motility mutants in three animal models. *Infect Immun*. 1991;59(8):2727-36.

6. **Watnick PI, Kolter R**. Steps in the development of a *Vibrio cholerae* El Tor biofilm. *Mol Microbiol*. 1999;34(3):586-95.

7. **Srivastava D, Harris RC, Waters CM**. Integration of cyclic di-GMP and quorum sensing in the control of vpsT and aphA in *Vibrio cholerae*. *J Bacteriol*. 2011;193(22):6331-41.

8. **Kaper JB, Morris JG, Jr., Levine MM**. Cholera. *Clin Microbiol Rev*. 1995;8(1):48-86.

9. **Wernick NL, Chinnapen DJ, Cho JA, Lencer WI**. Cholera toxin: an intracellular journey into the cytosol by way of the endoplasmic reticulum. *Toxins* (Basel). 2010;2(3):310-25.

10. **Herrington DA, Hall RH, Losonsky G, Mekalanos JJ, Taylor RK, Levine MM**. Toxin, toxin-coregulated pili, and the toxR regulon are essential for *Vibrio cholerae* pathogenesis in humans. *J Exp Med*. 1988;168(4):1487-92.

11. **Karatan E, Watnick P**. Signals, regulatory networks, and materials that build and break bacterial biofilms. *Microbiol Mol Biol Rev*. 2009;73(2):310-47.

12. **Donlan RM, Costerton JW**. Biofilms: survival mechanisms of clinically relevant microorganisms. *Clin Microbiol Rev*. 2002;15(2):167-93.

13. **Zhu J, Mekalanos JJ**. Quorum sensing-dependent biofilms enhance colonization in *Vibrio cholerae*. Dev Cell. 2003;5(4):647-56.

14. **Elasri MO, Miller RV**. Study of the response of a biofilm bacterial community to UV radiation. *Appl Environ Microbiol*. 1999;65(5):2025-31.

15. **Costerton JW, Cheng KJ, Geesey GG, Ladd TI, Nickel JC, Dasgupta M, et al**. Bacterial biofilms in nature and disease. *Annu Rev Microbiol*. 1987;41:435-64.

16. **Costerton JW, Lewandowski Z, Caldwell DE, Korber DR, Lappin-Scott HM**. Microbial biofilms. *Annu Rev Microbiol*. 1995;49:711-45.

17. **Tamayo R, Patimalla B, Camilli A**. Growth in a biofilm induces a hyperinfectious phenotype in *Vibrio cholerae*. *Infect Immun*. 2010;78(8):3560-9.

18. **Tischler AD, Camilli A**. Cyclic diguanylate (c-di-GMP) regulates *Vibrio cholerae* biofilm formation. *Mol Microbiol*. 2004;53(3):857-69.

19. **Romling U, Galperin MY, Gomelsky M.** Cyclic di-GMP: the first 25 years of a universal bacterial second messenger. *Microbiol Mol Biol Rev*. 2013;77(1):1-52.

20. **Romling U, Gomelsky M, Galperin MY**. C-di-GMP: the dawning of a novel bacterial signalling system. *Mol Microbiol*. 2005;57(3):629-39.

21. **Beyhan S, Odell LS, Yildiz FH**. Identification and characterization of cyclic diguanylate signaling systems controlling rugosity in *Vibrio cholerae*. *J Bacteriol*. 2008;190(22):7392-405.

22. **Tabor CW, Tabor H**. Polyamines. *Annu Rev Biochem*. 1984;53:749-90.

23. **Tabor CW, Tabor H**. Polyamines in microorganisms. *Microbiol Rev*. 1985;49(1):81-99.

24. **Karatan E, Duncan TR, Watnick PI**. NspS, a predicted polyamine sensor, mediates activation of *Vibrio cholerae* biofilm formation by norspermidine. *J Bacteriol*. 2005;187(21):7434-43.

25. **McGinnis MW, Parker ZM, Walter NE, Rutkovsky AC, Cartaya-Marin C, Karatan E**. Spermidine regulates *Vibrio cholerae* biofilm formation via transport and signaling pathways. *FEMS Microbiol Lett*. 2009;299(2):166-74.

26. **Cockerell SR, Rutkovsky AC, Zayner JP, Cooper RE, Porter LR, Pendergraft SS, et al.** *Vibrio cholerae* NspS, a homologue of ABC-type periplasmic solute binding proteins, facilitates transduction of polyamine signals independent of their transport. *Microbiology*. 2014;160(Pt 5):832-43.

27. **Sobe RC, Bond WG, Wotanis CK, Zayner JP, Burriss MA, Fernandez N, et al.** Spermine inhibits *Vibrio cholerae* biofilm formation through the NspS-MbaA polyamine signaling system. *J Biol Chem*. 2017;292(41):17025-36.

28. **Zappia V, Porta R, Carteni-Farina M, De Rosa M, Gambacorta A**. Polyamine distribution in eukaryotes: occurrence of sym-norm-spermidine and sym-nor-spermine in arthropods. *FEBS Lett*. 1978;94(1):161-5.

29. **Yamamoto S, Shinoda S, Kawaguchi M, Wakamatsu K, Makita M**. Polyamine Distribution in *Vibrionaceae* - Norspermidine as a General Constituent of *Vibrio* Species. *Can J Microbiol*. 1983;29(6):724-8.

30. **Hamana K, Matsuzaki S**. Widespread occurrence of norspermidine and norspermine in eukaryotic algae. *J Biochem*. 1982;91(4):1321-8.

31. **Stillway LW, Walle T**. Identification of the unusual polyamines 3,3'-diaminodipropylamine and N,N'-bis(3-aminoproply)-1,3-propanediamine in the white shrimp *Penaeus setiferus*. *Biochem Biophys Res Commun*. 1977;77(3):1103-7. doi:

32. **Michael AJ**. Polyamines in Eukaryotes, Bacteria, and Archaea. *J Biol Chem*. 2016;291(29):14896-903.

33. **Milovic V**. Polyamines in the gut lumen: bioavailability and biodistribution. *Eur J Gastroen Hepat*. 2001;13(9):1021-5.

34. **Murphy GM**. Polyamines in the human gut. *Eur J Gastroen Hepat*. 2001;13(9):1011-4.

35. **Matsumoto M, Kibe R, Ooga T, Aiba Y, Kurihara S, Sawaki E, et al**. Impact of intestinal microbiota on intestinal luminal metabolome. *Sci Rep*. 2012;2:233.

36. **Bomchil N, Watnick P, Kolter R**. Identification and characterization of a *Vibrio cholerae* gene, *mbaA*, involved in maintenance of biofilm architecture. *J Bacteriol*. 2003;185(4):1384-90.

37. **Zayner JP**. The Regulation of *Vibrio cholerae* Biofilm by NSPS and MBAA. Master's Thesis: Appalachian State University; 2008.

38. **Waldor MK, Mekalanos JJ**. Emergence of a new cholera pandemic: molecular analysis of virulence determinants in *Vibrio cholerae* O139 and development of a live vaccine prototype. *J Infect Dis*. 1994;170(2):278-83.

39. **O'Toole GA**. Microtiter dish biofilm formation assay. *J Vis Exp*. 2011(47).

40. **Kelley LA, Mezulis S, Yates CM, Wass MN, Sternberg MJ**. The Phyre2 web portal for protein modeling, prediction and analysis. *Nat Protoc*. 2015;10(6):845-58.

41. **Goddard TD, Huang CC, Meng EC, Pettersen EF, Couch GS, Morris JH, et al**. UCSF ChimeraX: Meeting modern challenges in visualization and analysis. *Protein Sci*. 2018;27(1):14-25.

42. **Combet C, Blanchet C, Geourjon C, Deleage G**. NPS@: network protein sequence analysis. *Trends Biochem Sci*. 2000;25(3):147-50.

43. **Thompson JD, Higgins DG, Gibson TJ.** CLUSTAL W: improving the sensitivity of progressive multiple sequence alignment through sequence weighting, position-specific gap penalties and weight matrix choice. *Nucleic Acids Res*. 1994;22(22):4673-80.

44. **Robert X, Gouet P**. Deciphering key features in protein structures with the new ENDscript server. *Nucleic Acids Res*. 2014;42(Web Server issue):W320-4.

45. **Neiditch MB, Federle MJ, Miller ST, Bassler BL, Hughson FM**. Regulation of LuxPQ receptor activity by the quorum-sensing signal autoinducer-2. *Mol Cell*. 2005;18(5):507-18.

46. **Chatterjee D, Cooley RB, Boyd CD, Mehl RA, O'Toole GA, Sondermann H**. Mechanistic insight into the conserved allosteric regulation of periplasmic proteolysis by the signaling molecule cyclic-di-GMP. *Elife*. 2014;3:e03650.

Appendix A: Supplemental Figures

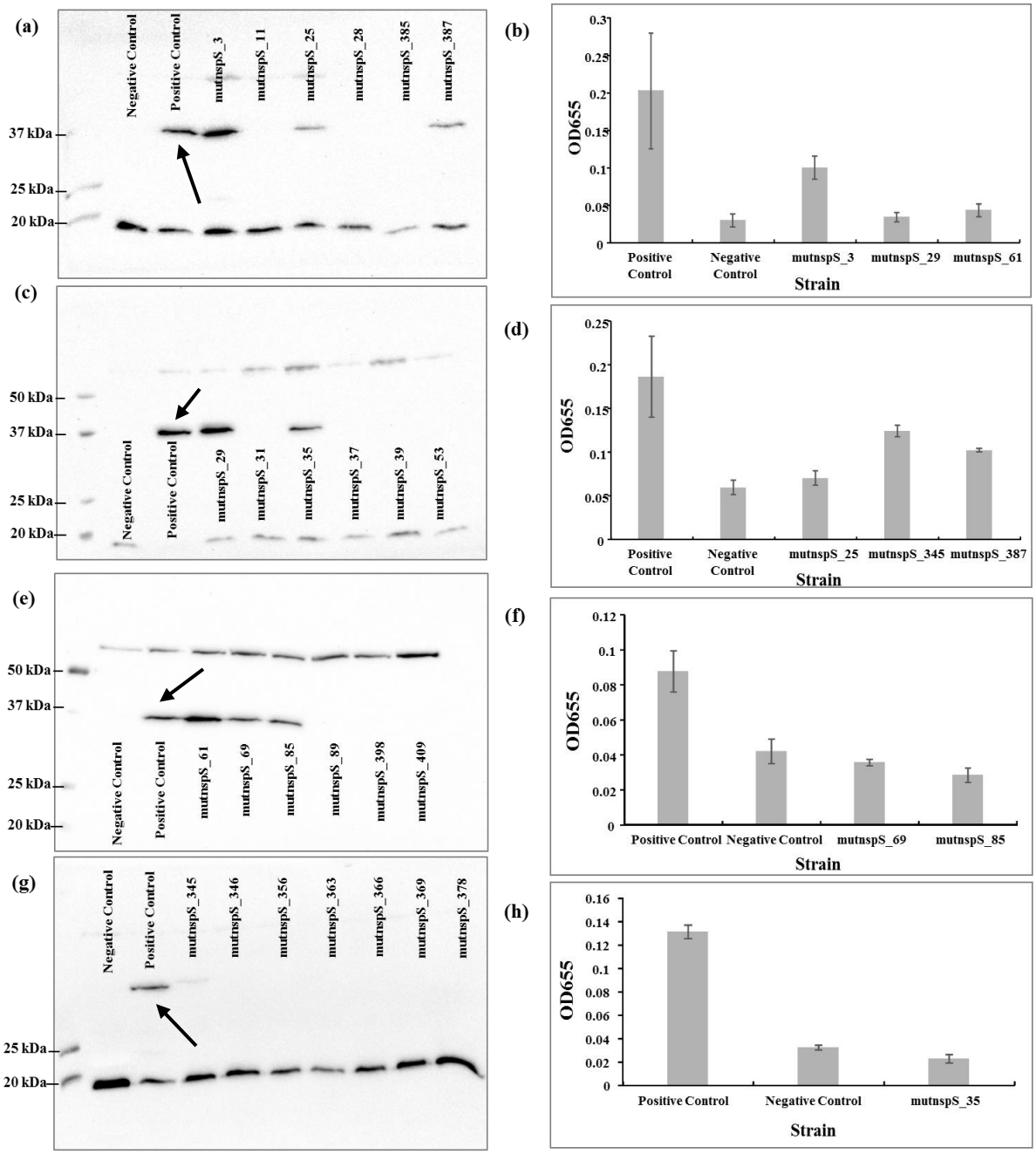

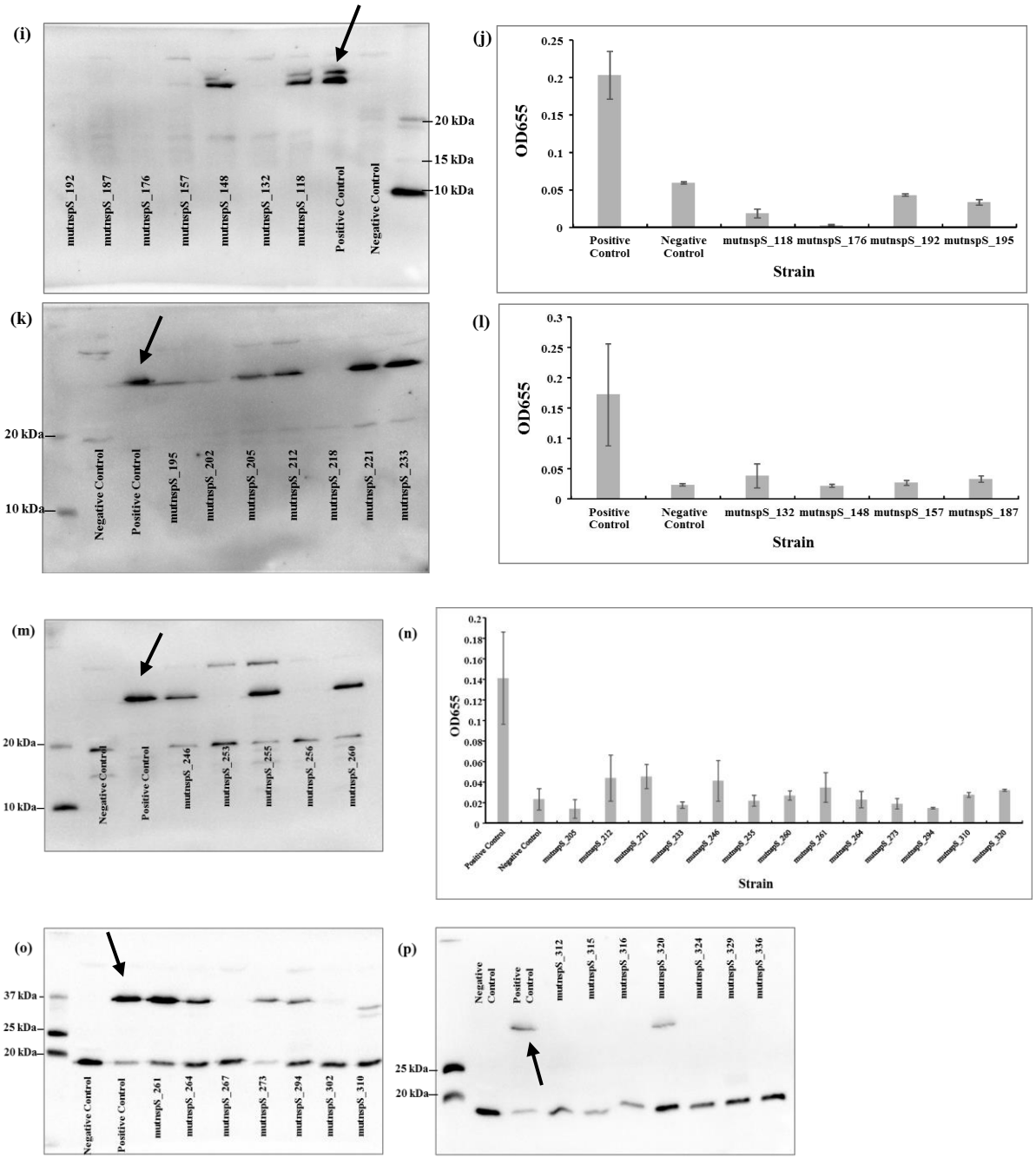
(i)
mutnspS_192
mutnspS_187
mutnspS_176
mutnspS_157
mutnspS_148
mutnspS_132
mutnspS_118
Positive Control
Negative Control
20 kDa
15 kDa
10 kDa
(j)
OD655
0.25
0.2
0.15
0.1
0.05
0
Positive Control
Negative Control
mutnspS_118
mutnspS_176
mutnspS_192
mutnspS_195
Strain
(k)
20 kDa
10 kDa
Negative Control
Positive Control
mutnspS_195
mutnspS_202
mutnspS_205
mutnspS_212
mutnspS_218
mutnspS_221
mutnspS_233
(l)
OD655
0.3
0.25
0.2
0.15
0.1
0.05
0
Positive Control
Negative Control
mutnspS_132
mutnspS_148
mutnspS_157
mutnspS_187
Strain
(m)
20 kDa
10 kDa
Negative Control
Positive Control
mutnspS_246
mutnspS_253
mutnspS_255
mutnspS_256
mutnspS_260
(n)
OD655
0.2
0.18
0.16
0.14
0.12
0.1
0.08
0.06
0.04
0.02
0
Positive Control
Negative Control
mutnspS_205
mutnspS_212
mutnspS_221
mutnspS_233
mutnspS_246
mutnspS_255
mutnspS_260
mutnspS_261
mutnspS_264
mutnspS_273
mutnspS_294
mutnspS_310
mutnspS_320
Strain
(o)
37 kDa
25 kDa
20 kDa
Negative Control
Positive Control
mutnspS_261
mutnspS_264
mutnspS_267
mutnspS_273
mutnspS_294
mutnspS_302
mutnspS_310
(p)
Negative Control
Positive Control
mutnspS_312
mutnspS_315
mutnspS_316
mutnspS_320
mutnspS_324
mutnspS_329
mutnspS_336
25 kDa
20 kDa

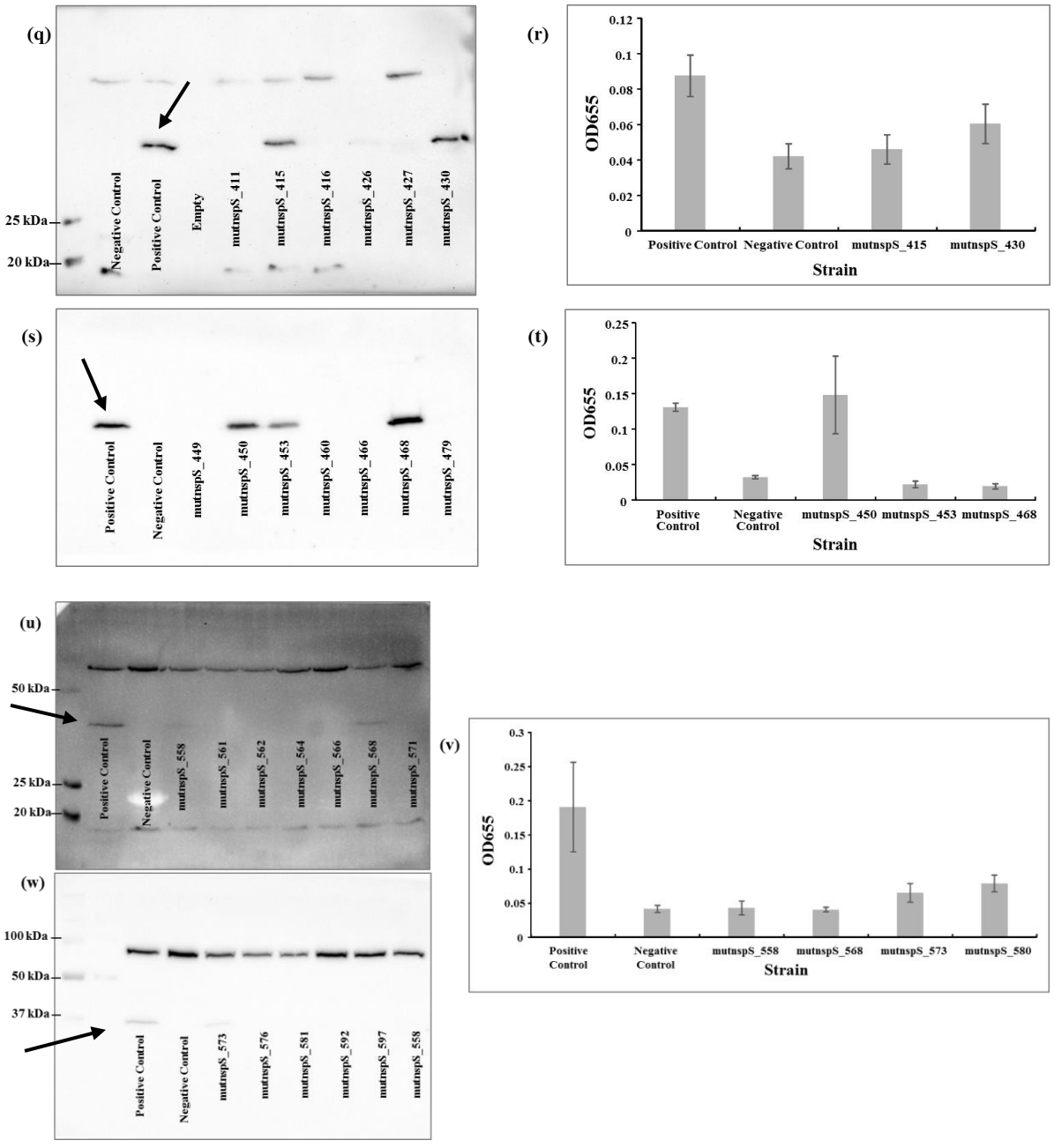
(q)
25 kDa
20 kDa
Negative Control
Positive Control
Empty
mutnspS_411
mutnspS_415
mutnspS_416
mutnspS_426
mutnspS_427
mutnspS_430
(r)
OD655
0.12
0.1
0.08
0.06
0.04
0.02
0
Positive Control
Negative Control
mutnspS_415
mutnspS_430
Strain
(s)
Positive Control
Negative Control
mutnspS_449
mutnspS_450
mutnspS_453
mutnspS_460
mutnspS_466
mutnspS_468
mutnspS_479
(t)
OD655
0.25
0.2
0.15
0.1
0.05
0
Positive Control
Negative Control
mutnspS_450
mutnspS_453
mutnspS_468
Strain
(u)
50 kDa
25 kDa
20 kDa
Positive Control
Negative Control
mutnspS_558
mutnspS_561
mutnspS_562
mutnspS_564
mutnspS_566
mutnspS_568
mutnspS_571
(v)
OD655
0.3
0.25
0.2
0.15
0.1
0.05
0
Positive Control
Negative Control
mutnspS_558
mutnspS_568
mutnspS_573
mutnspS_580
Strain
(w)
100 kDa
50 kDa
37 kDa
Positive Control
Negative Control
mutnspS_573
mutnspS_576
mutnspS_581
mutnspS_592
mutnspS_597
mutnspS_558

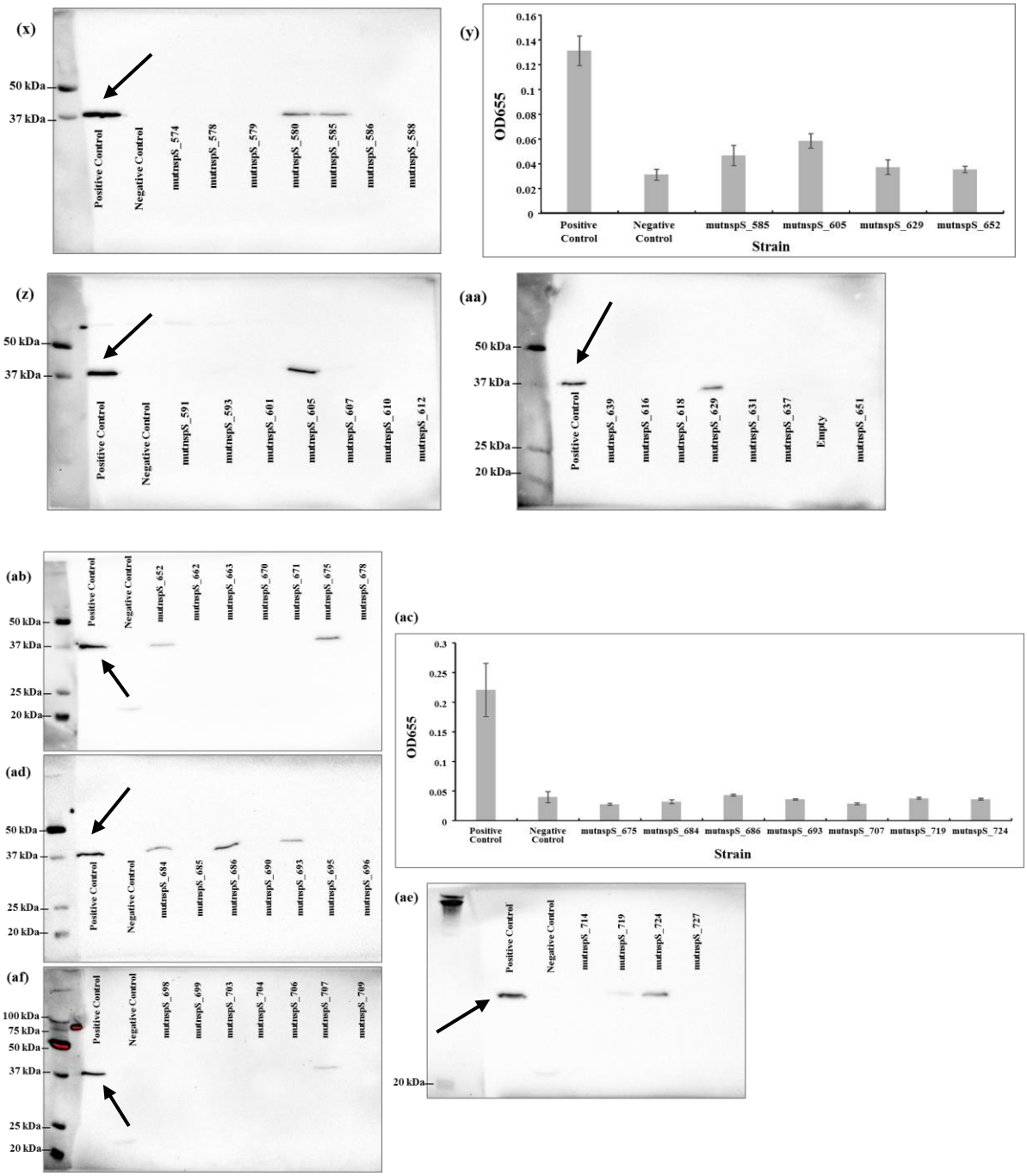
(x)
50 kDa
37 kDa
Positive Control
Negative Control
mutnspS_574
mutnspS_578
mutnspS_579
mutnspS_580
mutnspS_585
mutnspS_586
mutnspS_588
(y)
OD655
0.16
0.14
0.12
0.1
0.08
0.06
0.04
0.02
0
Positive Control
Negative Control
mutnspS_585
mutnspS_605
mutnspS_629
mutnspS_652
Strain
(z)
50 kDa
37 kDa
Positive Control
Negative Control
mutnspS_591
mutnspS_593
mutnspS_601
mutnspS_605
mutnspS_607
mutnspS_610
mutnspS_612
(aa)
50 kDa
37 kDa
25 kDa
20 kDa
Positive Control
mutnspS_639
mutnspS_616
mutnspS_618
mutnspS_629
mutnspS_631
mutnspS_637
Empty
mutnspS_651
(ab)
50 kDa
37 kDa
25 kDa
20 kDa
Positive Control
Negative Control
mutnspS_652
mutnspS_662
mutnspS_663
mutnspS_670
mutnspS_671
mutnspS_675
mutnspS_678
(ac)
OD655
0.3
0.25
0.2
0.15
0.1
0.05
0
Positive Control
Negative Control
mutnspS_675
mutnspS_684
mutnspS_686
mutnspS_693
mutnspS_707
mutnspS_719
mutnspS_724
Strain
(ad)
50 kDa
37 kDa
25 kDa
20 kDa
Positive Control
Negative Control
mutnspS_684
mutnspS_685
mutnspS_686
mutnspS_690
mutnspS_693
mutnspS_695
mutnspS_696
(ae)
20 kDa
Positive Control
Negative Control
mutnspS_714
mutnspS_719
mutnspS_724
mutnspS_727
(af)
100 kDa
75 kDa
50 kDa
37 kDa
25 kDa
20 kDa
Positive Control
Negative Control
mutnspS_698
mutnspS_699
mutnspS_703
mutnspS_704
mutnspS_706
mutnspS_707
mutnspS_709

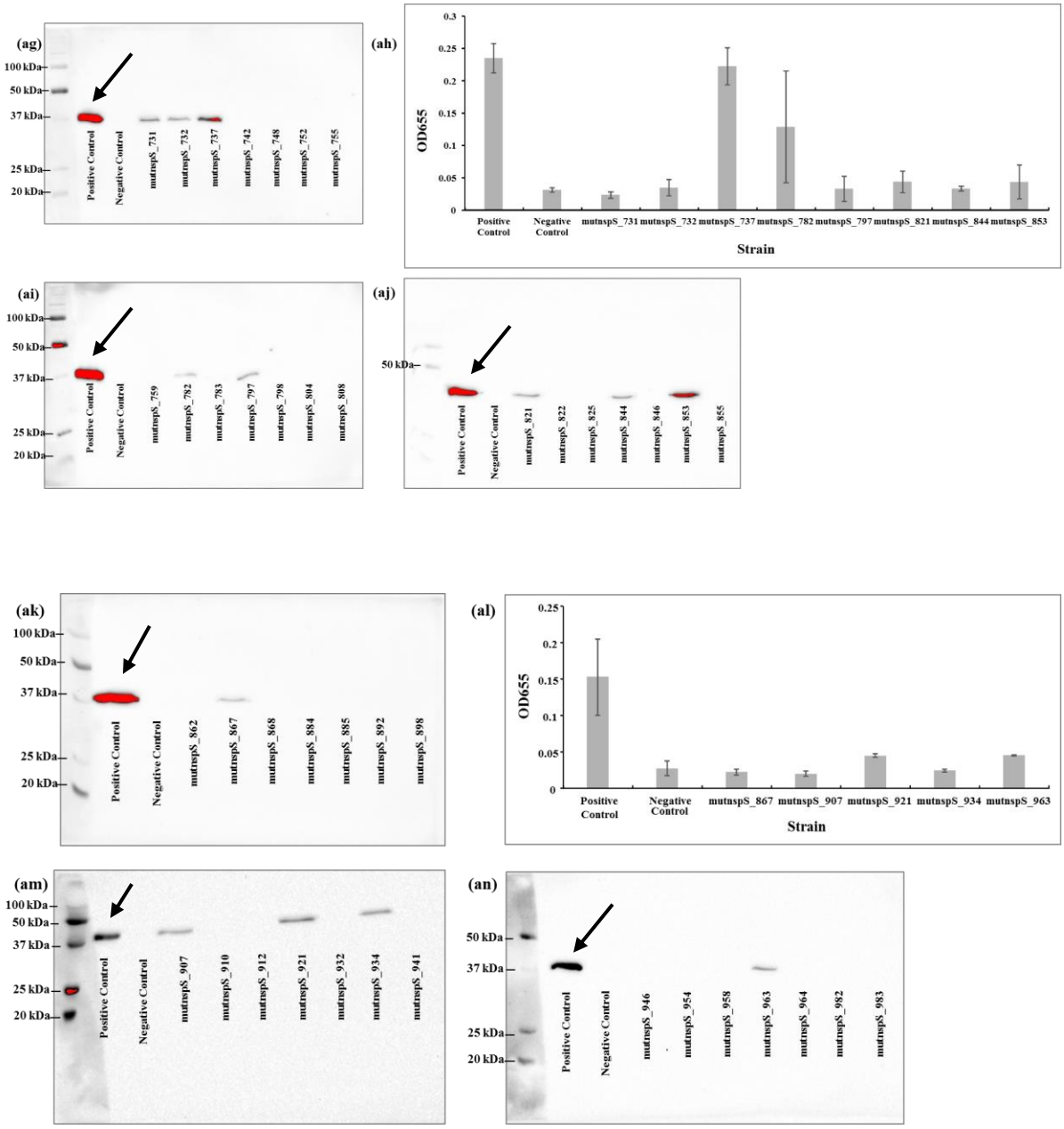
(ag)
100 kDa
50 kDa
37 kDa
25 kDa
20 kDa
Positive Control
Negative Control
mutnspS_731
mutnspS_732
mutnspS_737
mutnspS_742
mutnspS_748
mutnspS_752
mutnspS_755
(ah)
OD655
0.3
0.25
0.2
0.15
0.1
0.05
0
Positive Control
Negative Control
mutnspS_731
mutnspS_732
mutnspS_737
mutnspS_782
mutnspS_797
mutnspS_821
mutnspS_844
mutnspS_853
Strain
(ai)
100 kDa
50 kDa
37 kDa
25 kDa
20 kDa
Positive Control
Negative Control
mutnspS_759
mutnspS_782
mutnspS_783
mutnspS_797
mutnspS_798
mutnspS_804
mutnspS_808
(aj)
50 kDa
Positive Control
Negative Control
mutnspS_821
mutnspS_822
mutnspS_825
mutnspS_844
mutnspS_846
mutnspS_853
mutnspS_855
(ak)
100 kDa
50 kDa
37 kDa
25 kDa
20 kDa
Positive Control
Negative Control
mutnspS_862
mutnspS_867
mutnspS_868
mutnspS_884
mutnspS_885
mutnspS_892
mutnspS_898
(al)
OD655
0.25
0.2
0.15
0.1
0.05
0
Positive Control
Negative Control
mutnspS_867
mutnspS_907
mutnspS_921
mutnspS_934
mutnspS_963
Strain
(am)
100 kDa
50 kDa
37 kDa
25 kDa
20 kDa
Positive Control
Negative Control
mutnspS_907
mutnspS_910
mutnspS_912
mutnspS_921
mutnspS_932
mutnspS_934
mutnspS_941
(an)
50 kDa
37 kDa
25 kDa
20 kDa
Positive Control
Negative Control
mutnspS_946
mutnspS_954
mutnspS_958
mutnspS_963
mutnspS_964
mutnspS_982
mutnspS_983

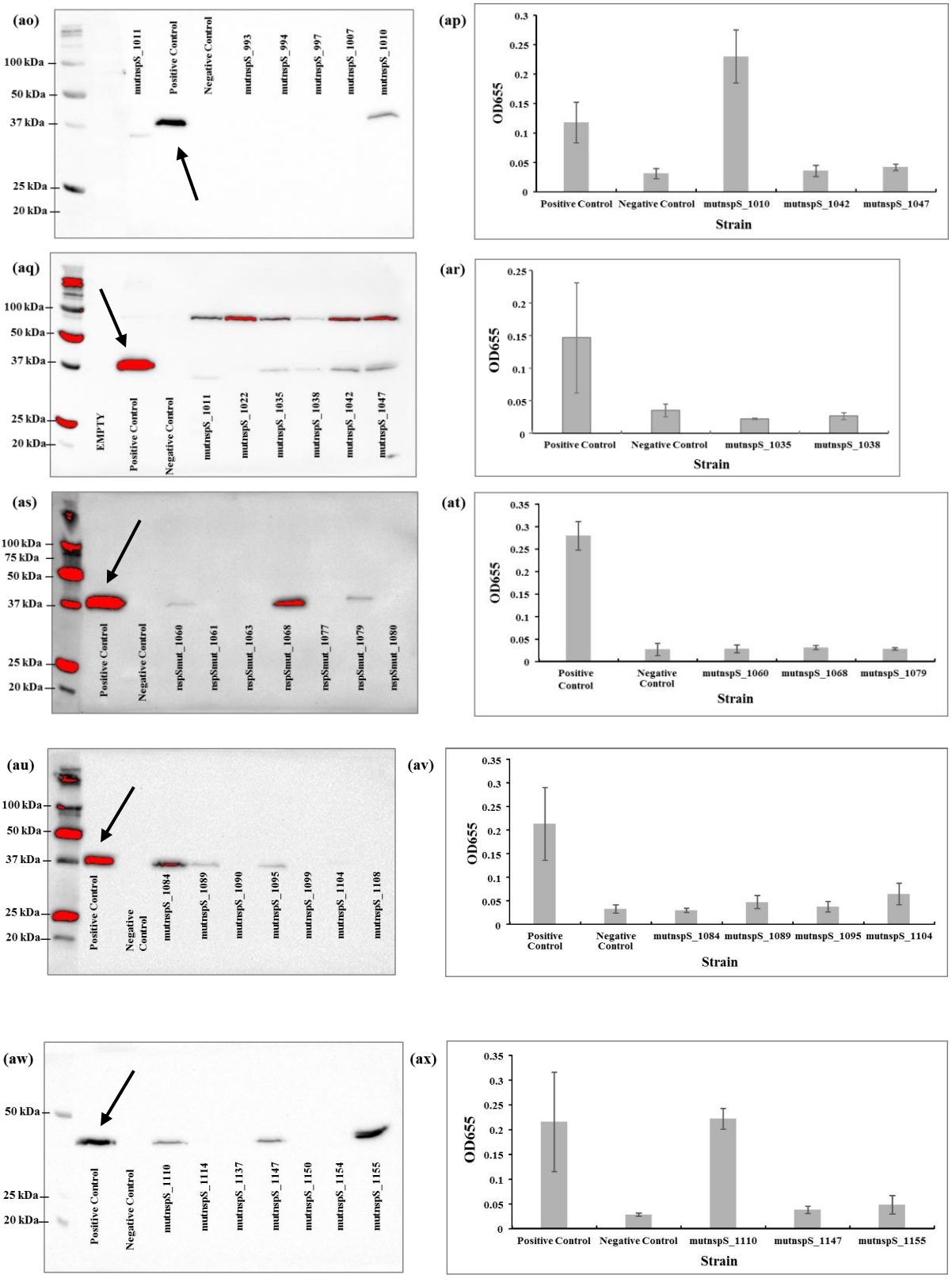
(ao)
100 kDa
50 kDa
37 kDa
25 kDa
20 kDa
mutnspS_1011
Positive Control
Negative Control
mutnspS_993
mutnspS_994
mutnspS_997
mutnspS_1007
mutnspS_1010
(ap)
OD655
0.3
0.25
0.2
0.15
0.1
0.05
0
Positive Control
Negative Control
mutnspS_1010
mutnspS_1042
mutnspS_1047
Strain
(aq)
100 kDa
50 kDa
37 kDa
25 kDa
20 kDa
EMPTY
Positive Control
Negative Control
mutnspS_1011
mutnspS_1022
mutnspS_1035
mutnspS_1038
mutnspS_1042
mutnspS_1047
(ar)
OD655
0.25
0.2
0.15
0.1
0.05
0
Positive Control
Negative Control
mutnspS_1035
mutnspS_1038
Strain
(as)
100 kDa
75 kDa
50 kDa
37 kDa
25 kDa
20 kDa
Positive Control
Negative Control
nspSmut_1060
nspSmut_1061
nspSmut_1063
nspSmut_1068
nspSmut_1077
nspSmut_1079
nspSmut_1080
(at)
OD655
0.35
0.3
0.25
0.2
0.15
0.1
0.05
0
Positive Control
Negative Control
mutnspS_1060
mutnspS_1068
mutnspS_1079
Strain
(au)
100 kDa
50 kDa
37 kDa
25 kDa
20 kDa
Positive Control
Negative Control
mutnspS_1084
mutnspS_1089
mutnspS_1090
mutnspS_1095
mutnspS_1099
mutnspS_1104
mutnspS_1108
(av)
OD655
0.35
0.3
0.25
0.2
0.15
0.1
0.05
0
Positive Control
Negative Control
mutnspS_1084
mutnspS_1089
mutnspS_1095
mutnspS_1104
Strain
(aw)
50 kDa
25 kDa
20 kDa
Positive Control
Negative Control
mutnspS_1110
mutnspS_1114
mutnspS_1137
mutnspS_1147
mutnspS_1150
mutnspS_1154
mutnspS_1155
(ax)
OD655
0.35
0.3
0.25
0.2
0.15
0.1
0.05
0
Positive Control
Negative Control
mutnspS_1110
mutnspS_1147
mutnspS_1155
Strain

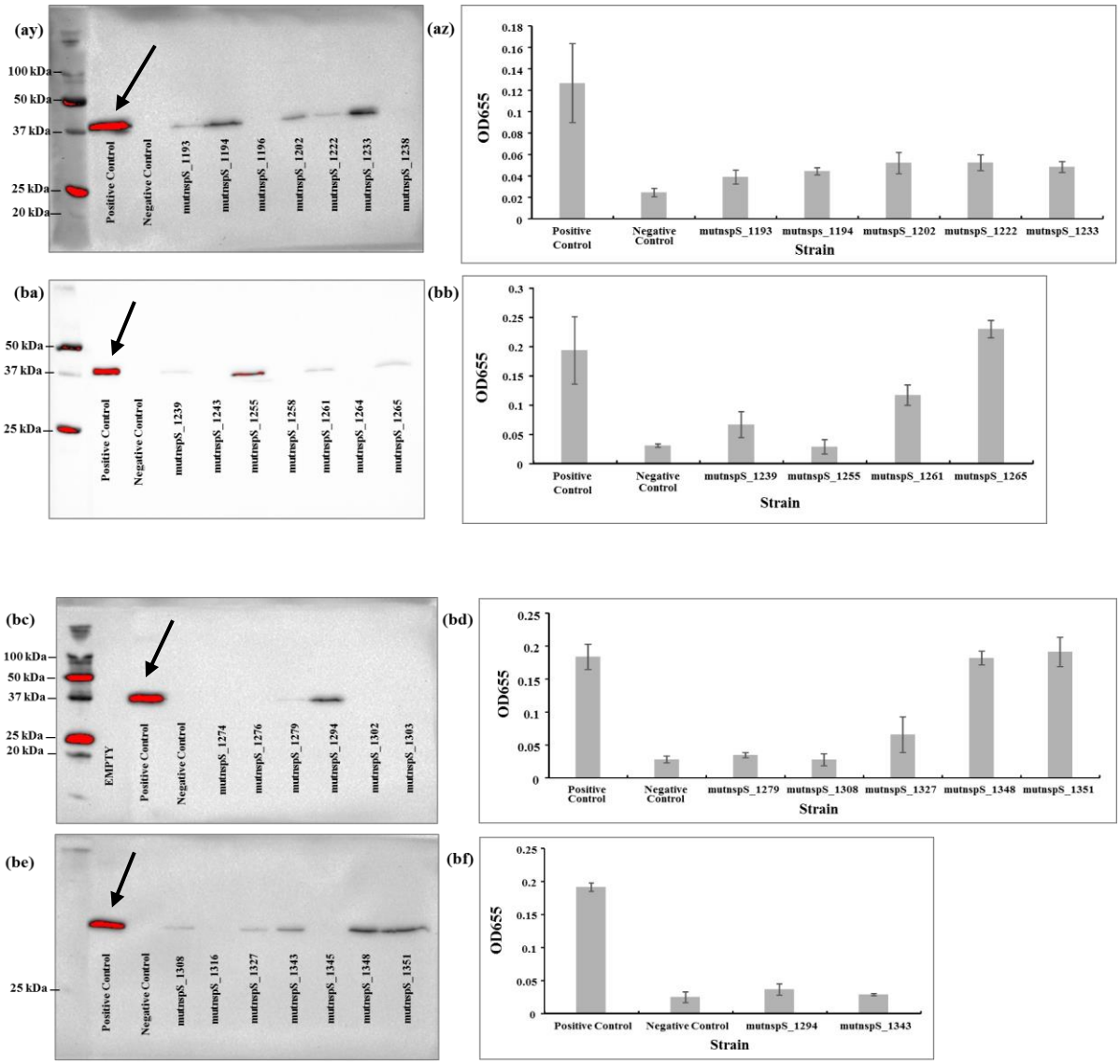
(ay)
100 kDa
50 kDa
37 kDa
25 kDa
20 kDa
Positive Control
Negative Control
mutnspS_1193
mutnspS_1194
mutnspS_1196
mutnspS_1202
mutnspS_1222
mutnspS_1233
mutnspS_1238
(az)
OD655
Positive Control
Negative Control
mutnspS_1193
mutnspS_1194
mutnspS_1202
mutnspS_1222
mutnspS_1233
Strain
(ba)
50 kDa
37 kDa
25 kDa
Positive Control
Negative Control
mutnspS_1239
mutnspS_1243
mutnspS_1255
mutnspS_1258
mutnspS_1261
mutnspS_1264
mutnspS_1265
(bb)
OD655
Positive Control
Negative Control
mutnspS_1239
mutnspS_1255
mutnspS_1261
mutnspS_1265
Strain
(bc)
100 kDa
50 kDa
37 kDa
25 kDa
20 kDa
EMPTY
Positive Control
Negative Control
mutnspS_1274
mutnspS_1276
mutnspS_1279
mutnspS_1294
mutnspS_1302
mutnspS_1303
(bd)
OD655
Positive Control
Negative Control
mutnspS_1279
mutnspS_1308
mutnspS_1327
mutnspS_1348
mutnspS_1351
Strain
(be)
25 kDa
Positive Control
Negative Control
mutnspS_1308
mutnspS_1316
mutnspS_1327
mutnspS_1343
mutnspS_1345
mutnspS_1348
mutnspS_1351
(bf)
OD655
Positive Control
Negative Control
mutnspS_1294
mutnspS_1343
Strain

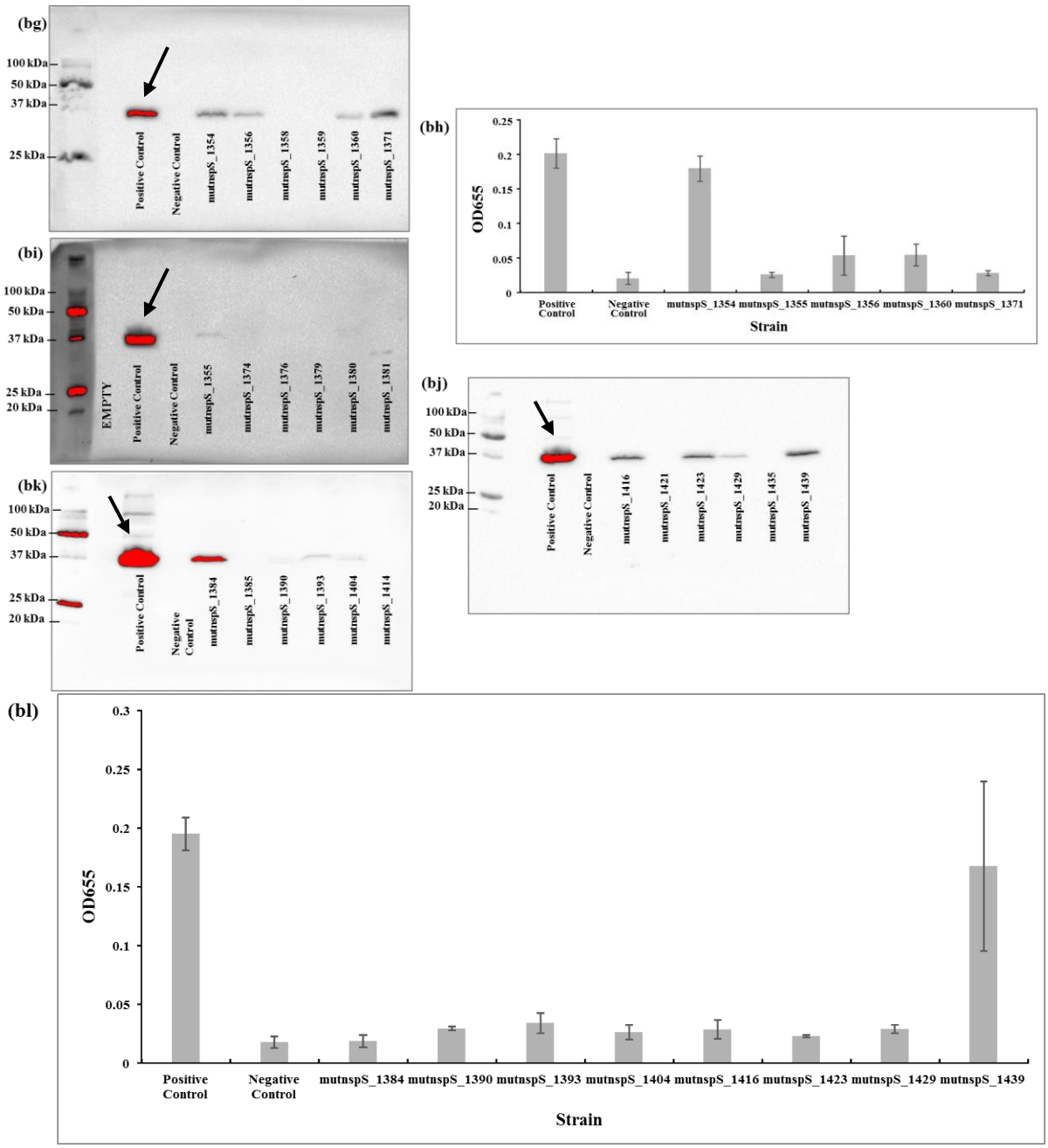

Figure S1. **Analysis of NspS protein expression and tertiary screen of biofilm formation for mutant clones**. (a-bl) Western blots with corresponding final biofilm formation analysis for the mutant clones that showed low biofilm formation in the first and second screens. For western blots with the exception of (i) and (s), the ladder is in Lane 1 or 2. For (i), the ladder is in Lane 10. For (s), the ladder did not image well enough to be seen on the western. An arrow points to the NspS band in the positive control lane in each of the western blots. All western blot images were taken with a BIO-RAD Molecular Imager Gel Doc XR System. For all figures, the positive control is *V. cholerae* Δ*nspS* with pACYC184::*nspS*-V5 and the negative control is *V. cholerae* Δ*nspS* with pACYC184. For biofilm graphs, three biological replicates were analyzed in triplicate per mutant clone for biofilm formation. Error bars show standard deviations of three biological replicates.

Vita

Erin Campbell Young was born in Charlotte, North Carolina and graduated from Butler High School in Matthews, North Carolina. She received her Bachelor of Science in Biology with minors in French, Spanish and Chemistry from the University of North Carolina at Chapel Hill in May 2010. She spent several years working in research labs at Duke University and North Carolina State University before entering the master's program at Appalachian State and joining Dr. Ece Karatan's lab in August 2017. After receiving her Master of Science degree in Cell and Molecular Biology from Appalachian State in August 2019, she will pursue a career in science.